Pliocene onset of rapid exhumation in Taiwan during arc-continent collision: new insights from detrital thermochronometry

Cite As: Kirstein, LA, Fellin, MG, Willett, SD, Carter, A, Chen, Y-G, Garver, JI & Lee, DC 2010, 'Pliocene onset of rapid exhumation in Taiwan during arc-continent collision: new insights from detrital thermochronometry' *Basin Research*, vol 22, no. 3, pp. 270-285.

Onset of rapid exhumation in Taiwan during the Pliocene constrained by detrital thermochronometry

L.A. Kirstein[a], M.G. Fellin[b], S.D. Willett[b], A. Carter[c], Y-G. Chen[d], J.I.Garver[e], D.C. Lee[f]

[a] School of GeoSciences, University of Edinburgh, Edinburgh, EH9 3JW, U.K. (linda.kirstein@ed.ac.uk)

[b]ETH Zürich, Department of Earth Sciences, CH8092 Zurich, Switzerland

[c]School of Earth Sciences, Birkbeck College, University of London, London, WC1E 7HX, U.K. (a.carter@ucl.ac.uk)

[d] Department of Geosciences, National Taiwan University, No.1, sec. 4th, Roosevelt Road, Taipei 10617, Taiwan, ROC. (ygchen@ntu.edu.tw)

[e]Department of Geology, Olin Building, Union College, 807 Union St., Schenectady, NY 12308-2311, USA (garverj@union.edu)

[f] Institute of Earth Sciences, Academia Sinica, 128 Academia Road, Nankang, Taipei 115, Taiwan, ROC. (dclee@earth.sinica.edu.tw)

ABSTRACT

The Coastal Range in eastern Taiwan contains the remnants of the Pliocene-Pleistocene retro-foredeep basin of the ongoing Penglai orogeny. These sedimentary successions record the earliest exhumation of the Central Range, Taiwan. We dated detrital Plio-Pleistocene sediments in the Coastal Range using multiple thermochronometers (zircon fission-track, zircon (U-Th)/He and U/Pb dating) to reveal changes in exhumation rate through time. These chronometers record an increase in exhumation rate between 5 and 3 Ma that is first detected in sediments deposited at ~1.9 Ma. Based on detrital thermochronometry and assuming arc-continent collision occurred in the late Miocene (~6.5 Ma) the exhumational history of Taiwan can be subdivided in two stages: a first stage of low exhumation rate from the late Miocene to the early Pliocene; and a second stage of high exhumation rate of ~4 mm/yr from 5-3 Ma to Present. The onset of high exhumation rates occurred at the same time as other major tectonic changes including an increase in subsidence rate in both the pro- and retro-foredeep basins, and a change in the wedge kinematics from internal shortening to underplating. These changes may be related to progressive thickening of the wedge and a change in the critical taper during arc-continent collision resulting in topographic growth with consequent increased erosion rates.

1. INTRODUCTION

Taiwan has evolved through time from an intra-oceanic subduction zone with a volcanic arc and submarine accretionary wedge, to a subaerial double-

vergent orogen involving continental basement rocks (Davis *et al.*, 1983; Lundberg *et al.*, 1997; Fuller *et al.*, 2006; Fisher *et al.*, 2007). This is the result of closure of the South China Sea by subduction of the oceanic crust and the convergence between the Eurasian continental margin and the Luzon arc during the late Miocene-early Pliocene (Suppe, 1984; Liu *et al.*, 2001; Lin *et al.* 2003; Fuller *et al.*, 2006). Currently Taiwan is a rapidly evolving orogen with the most metamorphosed rocks exposed in the retrowedge, that is also the zone with the highest relief (>4 km; e.g. Fuller *et al.*, 2006). Based on apatite and zircon fission-track data, the metamorphosed rocks in Taiwan have experienced some of the highest long-term exhumation rates in the world (3-5 mm/yr, Liu *et al.,* 2000; Willett *et al.,* 2003; Fuller *et al.*, 2006; Lee *et al.*, 2006). Decadal-timescale sediment yield data (Li, 1976; Dadson *et al.*, 2003; 2004) and millennial timescale surface exposure dating by cosmogenic nuclides (Schaller *et al.*, 2005) record large spatial variations in erosion rate in response to recent earthquakes and localized weather events, but give an average erosion rate of about 5 mm/yr. All these studies show a general agreement between long-term and short-term exhumation rates suggesting that high exhumation rates at the scale of the orogen have been sustained for at least several million years (Dadson *et al.*, 2003). Whether these high exhumation rates observed today in Taiwan have been maintained since arc-continent collision is uncertain. For instance, zircon fission-track (ZFT) studies indicate that the onset of the modern high exhumation rates occurred only in the middle Pleistocene although regions in northern and southern Taiwan were cooling by about 5 Ma suggesting that some cooling, likely

caused by erosion, was already occurring in late Miocene time (Liu, 1988; Lee *et al.*, 2006). However, the sedimentary record of the retro-foredeep basin suggests that the onset of high exhumation rates might have occurred at about 3 Ma, when an increase of Taiwan-derived sediments entering the syncollisional basin is observed (Chi *et al.*, 1981).

In order to document the early exhumational history of Taiwan and the onset of high exhumation rates, we used a combination of detrital fission-track, (U-Th)/He and U-Pb dating on the sedimentary successions in the Coastal Range where remnants of the Plio-Pleistocene retro-foredeep basin are preserved. We focused on this area because, assuming a self-similar growth of the accretionary wedge, the retro-foredeep has likely received the first detritus from the metamorphic core of Taiwan. Moreover, while the foreland basin is the sink of sediments derived from both Taiwan and Eurasia, the retro-foredeep collected sediment sourced either from the Luzon arc or from Taiwan that produced clastics with very distinct compositional signatures (Teng, 1987; Dorsey & Lundberg, 1988; Dorsey, 1992). Finally, in the Coastal Range magneto-biostratigraphic data provide good constraints on the depositional ages of the syncollisional sediments (Chi *et al.*, 1981; Lee *et al.*, 1991; Horng *et al.*, 1999).

2. GEOLOGICAL SETTING

2.1 TECTONO-STRATIGRAPHIC UNITS

Taiwan is typically divided into a number of geologic provinces that include the foreland basin, the collisional orogenic belt and the remnant Luzon arc in the Coastal Range which makes up the focus of this study (Fig. 1).

The foreland basin consists of the coastal plains of western Taiwan and of the offshore Taiwan Strait (CP, Fig. 1). Seismic and well data from the Taiwan Strait show a regional basal unconformity that relates to the beginning of the foreland subsidence at about 6.5 Ma according to Lin *et al.* (2003). Foreland subsidence was initially slow but accelerated at 4 Ma with progressive advancement of the orogenic load onto the passive margin (Lin *et al.*, 2003).

Five major tectono-stratigraphic units form the collisional orogenic belt (Ho, 1999): the Western Foothills (WF), the Hengchun Peninsula (HP), the Hsuehshan Range (HR), the Backbone Slates (BS) and the Tananao Complex (TC) (Fig. 1). The Western Foothills correspond to a fold-and-thrust belt affecting non-metamorphic Oligocene-Pleistocene sediments (Suppe 1980 a,b). The Hengchun Peninsula is the emerged continuation of the submarine accretionary wedge south of Taiwan and it consists of Miocene-to-Pleistocene tectonic units that have suffered very-low grade metamorphism (Chang *et al.,* 2003). The Hsuehshan Range exposes Eocene to Oligocene meta-sediments originally deposited in the Eurasian passive margin during rifting and opening of the South China Sea. In the Hsuehshan Range detrital ZFT data record grain age variations that span the Oligocene to Carboniferous whereas thermally reset ZFT samples yield grain ages from 2.4 ± 1.0 to 8.7 ± 2.9 Ma giving central ages from 6.4 ± 1.6 to 2.9 ± 1.4 Ma (Fig. 2; Liu, 1988; Liu *et al.,* 2001). The Backbone Slates are

meta-sediments of Eocene to Miocene age that were deposited also in the passive margin and that stratigraphically overlie the Tananao Complex. The Backbone Slates have a ZFT age distribution similar to the Hsuehshan Range with both fully and partially annealed zircons and central ages from 6.0 ± 1.3 to 1.9 ± 0.7 Ma (Fig. 2; Liu *et al.*, 2001). The Tananao Complex is composed of highly deformed pre-Tertiary basement and it is the most metamorphosed portion of the belt with metamorphic facies up to upper greenschist (~500°C, Ernst & Jahn, 1987). This complex is exposed in the retro-wedge zone where ZFT ages are in the range 2.9 ± 1.3 to 0.8 ± 0.2 Ma (Fig. 2; Liu *et al.*, 2001; Willett *et al.*, 2003). The ensemble of the Hseuhshan Range, Tananao Complex and the Backbone Slates is commonly referred to as the Central Range (Ho, 1999) (Fig. 1).

The orogenic belt of Taiwan and the remnant of the Luzon arc are separated by the Longitudinal Valley that is filled with Pleistocene-Holocene clastics (Shyu *et al.*, 2005). To the east of this valley, the Coastal Range (CoR; Fig. 1) exposes Miocene arc-related volcanic rocks unconformably overlain by 5 to 6 km of Plio-Pleistocene syncollisional sediments (Dorsey & Lundberg, 1988; Lundberg & Dorsey, 1990). The oldest syn-collisional sediments are 4-5 Ma (Lower Pliocene, NN13-15; Chi *et al.*, 1981) and the basal unconformity shows a systematic decrease in age from early Pliocene in the WNW to early Pleistocene in the ESE (Dorsey, 1992). In Pliocene and early Pleistocene time the retro-foredeep basin was fully developed as an elongate marine basin dominated by a south-dipping tempestite-turbidite ramp (Dorsey & Lundberg, 1988). The

syncollsional sequence is subdivided into two formations: the Pliocene Fanshuliao Formation and the Plio-Plesitocene Paliwan Formation. The former is a sequence of turbidites composed of volcanic detritus, fossils and quartzo-feldspathic grains; whereas the latter contains turbidites dominated by metasedimentary rock fragments (Teng, 1987; Dorsey, 1988). The variety and composition of the lithic fragments in the Paliwan Formation records input from a source area with lower- and middle-greenschist facies rocks (Dorsey, 1988). Illite crystallinity data indicate that the geothermal gradient within the basin was ca. 14 °C/km and that the duration of burial diagenesis was less than 1 million years (Dorsey *et al.*, 1988).

2.2 TECTONO-METAMORPHIC EVOLUTION

The obliquity between the Luzon arc and the Eurasian margin resulted in the progressive southward propagation of arc-continent collision (Suppe, 1981). This complicates assigning an age to the onset of arc-continent collision, which is bracketed within a wide range of ages between 12 and 1 Ma (Suppe, 1984; Lu & Hsü, 1992; Byrne & Liu, 2002; Lin *et al.*, 2003; Lee *et al.*, 2006). The oldest estimate for the onset of arc-continent collision is based on palaeopositions of the Luzon arc-trench system (Teng, 1990) and on the change in the pole of rotation of the Philippine Sea Plate and the Eurasian Plate at 8 Ma (Sibuet *et al.,* 2002) with the assumption that collision and the change in the pole of rotation are related (Lee *et al.,* 1991). Based on time-space equivalence Suppe (1981) proposed that arc-continent collision occurred in the north of Taiwan in the

Pliocene (~4 Ma), while Yen (2003) favoured a model of two-stage collision with accretion of a rifted continental microplate during the Miocene.

In the modern foredeep west of Taiwan stratigraphic relationships record the end of the passive margin and onset of foreland-basin deposition due to onset of arc-continent collision at about 6.5 Ma (Lin *et al.,* 2003). Syn-collisional sediments of the retro-foredeep exposed in the Coastal Range date from the early Pliocene (~ 5 Ma, Dorsey & Lundberg, 1988), suggesting that a proto-Taiwan orogenic belt was exposed to erosion at least since early Pliocene time. Moreover, the decrease in age from WNW to ESE of the regional unconformity underlying these syncollisional sediments has been interpreted as related to the southward propagation of arc-continent collision and to the approach of the orogenic load towards the retro-foredeep basin (Chi *et al.*, 1981, Dorsey & Lundberg, 1988).

Zircon fission-track (ZFT) data from the Central Range including the Hsuehshan Range indicate that cooling from temperatures above 300 °C started around 5-6 Ma (Fig. 2; Liu *et al.*, 2001, Lee *et al.*, 2006). U-Th/He data on zircons and Raman spectrometry data on carbonaceous material coupled with wedge-kinematic modelling (Beyssac *et al.*; 2007) suggest that the high metamorphic temperatures of the Central Range Tananao Complex are related to the Taiwan orogeny, and that the distribution of metamorphic temperatures and cooling ages can be best reproduced by continuous underplating over the last 4 Myr (Beyssac *et al.*, 2007). Despite the wealth of geochronologic data, thermochronometers do not resolve well when the peak metamorphic event of the Penglai orogeny

occurred. The high metamorphic temperatures recorded in the Hsuehshan Range (345-475°C) are considered to have been acquired in the passive margin during rifting in the Oligocene (Beyssac *et al.*, 2007). Ar-Ar cooling ages from amphibole, muscovite and biotite have been measured on Mesozoic amphibolites and granitic rocks from the Tananao Complex (Lo & Onstott, 1995). Amphibole Ar-Ar cooling ages range from Cretaceous to Eocene (73-55 Ma) indicating that amphibole was not completely reset during the Penglai orogeny (Lo & Onstott, 1995). In some samples the low-temperature steps indicate a thermal overprint in the Miocene ~ 7.8 Ma (Lo & Onstott, 1995). Muscovite Ar-Ar cooling ages also show scatter and indicate cooling from the Cretaceous (85 Ma) to the Oligocene (25 Ma) (Lo & Onstott, 1995). As in the amphibole analyses, the lowest temperature steps indicate a late Tertiary (9-6 Ma) thermal event. Ar-Ar data on a fresh biotite separate from the Chipan area (Fig. 1) yielded an intercept age of 7.9 ± 0.1 Ma (Lo & Onstott, 1995). Finally, the main mylonitization phase in the Hoping gneiss is dated at 3-4 Ma using Ar-Ar in biotite (Wang *et al.*, 1998), indicating cooling from temperatures of <350°C during orogeny.

Based on the evidence outlined above, most workers currently believe that arc-continent collision in this region began in the late Miocene-early Pleistocene between 6.5 and 4 Ma. However, no evidence resolves consistently the onset of the high exhumation rates observed today.

3. SAMPLING STRATEGY AND ANALYTICAL TECHNIQUES

3.1 SAMPLING STRATEGY

We sampled four sections exposed at Shuilien, Hsiukuluan, Sanfu and Shuimuting that span a distance of ~50 km in the northern half of the Coastal Range where the oldest syncollisional sediments are preserved (Fig. 1) (Chi *et al.*, 1981, Dorsey, 1988). These sections reveal cycles of deposition with conglomerate, turbiditic sediments and deep-marine mudstone (Dorsey & Lundberg, 1988). The turbidite sandstone-siltstone units which potentially preserve suitably sized (>100 μm) apatite and zircon grains were sampled. Moreover, the sampled sections have relatively continuous bio- and magneto-stratigraphic records that provide good control on depositional ages (Chi *et al.*, 1981; Lee *et al.*, 1991).

Fourteen samples were collected that span a stratigraphic age range from the Pliocene to Pleistocene (4.1-0.8 Ma). Due to the short duration of orogenic processes in Taiwan, only highly sensitive thermochronometric systems can resolve potential temporal variations in erosion rates. Here ZFT dating of Plio-Pleistocene sediments is coupled with (U-Th)/He dating in selected samples to increase the accuracy of the cooling age measured. Since exhumation rates are high, a thermochronometer with a higher effective closure temperature should generate ages and lag times that are more sensitive to changes in erosion rate (Rahl *et al.*, 2007). However we attempted to date detrital apatite grains from these samples also to gain insight into the lower temperature cooling history. Finally in order to reveal possible syn-sedimentary volcanic sources and in general to better constrain the sedimentary source areas, U/Pb dating was undertaken.

3.2 SAMPLED SECTIONS

In the following section absolute ages of magnetic polarity chrons and biostratigraphic zones are based on Gradstein *et al.* (2004), and absolute ages for the sampled sections reported in previous studies have been converted according to this time scale.

The sampled section at Shuilien is exposed in the northern Coastal Range close to Shuilien Village and continues inland for ~2 km (Fig. 1). The lower part of the section contains thin to medium bedded turbidites consisting of inter-layered sandstone and mudstone of early-Pliocene age (Chi *et al.*, 1981), overlain by thick conglomerates that were deposited in a marginal-marine deltaic plain environment during late Pliocene time (Dorsey, 1988) (Fig. 3). The upper part of the section lacks a good age control, thus we sampled the early-Pliocene turbidites (SH4-SH6) that were deposited at 4.13-3.79 as inferred from palaeomagnetic and biostratigraphic data (NN14/15; C2Ar; Lee *et al.*, 1991) (Fig. 3).

To the south (Fig. 1), four sandstone (HK1-HK4) and one cobble (HK5) samples were collected from the sedimentary section along the Hsuikuluan River. HK1 is from the lowest part of the section that consists of thin bedded tempestites with sandy horizons, and that has a depositional age of 2.58-2.06 Ma (C2r; NN16-NN18; Lee *et al.*, 1991) (Fig. 3). HK4 and HK5 are from the middle part of the section where massive conglomerates are dominant and only locally interlayered with graded sandstone horizons (Fig. 3). HK4 is from a sandstone

horizon whereas HK5 is a schist cobble from a conglomerate, and their depositional age is 1.20-1.07 Ma (C1r.2r, NN19; Lee *et al.*, 1991). Finally two samples (HK2, HK3) are from medium bedded sandstone-siltstone turbidites towards the top of the sequence and were deposited between 0.99-0.78 Ma (C1r.1r, NN19; Lee *et al.*, 1991) (Fig. 3).

The Sanfu section is located 4 km south of the Hsuikuluan River (Fig. 1) and exposes a coarsening-upward sequence with mudstones at the base overlain by a 8-m thick pebbly mudstone, a first continuous turbiditic unit consisting of coarse-grained quartz-rich sandstones, a 30-m thick coarse sandstone with abundant small slate pebbles, and finally a second, strongly-deformed, turbiditic unit (Fig. 3). We collected three samples (40-01 to 42-01) from the portion of the first turbiditic unit that based on magneto- and biostratigraphic correlations is dated at 1.81-1.95 (C2n; NN18; Horng *et al.*, 1999) (Fig. 3). One sample (43-01) was collected from the second turbiditic sequence that has a depositional age younger than 1.77 Ma (Fig. 3).

Three samples were analyzed from the section at Shuimuting (Fig. 1) that has recently been the subject of a magneto-biostratigraphy study (C-S. Horng, pers.comm.). The section spans the transition between the arc-sourced sediments of the Fanshuliao Formation and the dominantly continental-sourced sediments of the Paliwan Formation. Sample SM1 is from a sandstone unit above the contact with the Kangkou limestone which contains volcanic and limestone fragments and it has a depositional age of 3.22-2.58 Ma (C2An) (Fig. 3). Up sequence, SM6 was selected from the sandstone-mudstone turbidites

deposited between 2.58 and 1.95 Ma (C2r) (Fig. 3). Finally, sample SM9 is from a siltstone-mudstone unit in the upper part of the section deposited between 1.95 and 1.77 Ma (C2n) (Fig. 3).

3.3 ANALYTICAL TECHNIQUES

Fission-track data were collected using the conventional external detector method (EDM). Apatite and zircon separates were prepared from the 100–150 μm fraction of each rock and analysed at University College London (UCL) or Union College (Schenectady, NY).

Several teflon grain mounts were made for each zircon sample and polished internal surfaces were etched in a eutectic of KOH:NaOH at 225-228°C for different periods of time (typically between 12 and 48 hrs) to ensure optimum etching of the different zircon populations. Apatite grain mounts were etched with 5N HNO3 at 20°C for 20 seconds. Samples analysed at University College London were irradiated in the well-thermalised (Cd ratio for Au >100) Hifar Reactor, at Lucas Heights in Australia and the FRM-II reactor at the University of München, Garching facility. Samples analysed at Union College were irradiated at the Triga Reactor, Oregon State University, USA. Measurement was made by optical microscopy using EDM with muscovite mica detectors. Corning glass CN2 (zircon) and CN5 (apatite) were used as a neutron flux monitor with dosimeters placed at each end of the sample stack to monitor for any flux gradients. Ages were calculated using the zeta method (Hurford & Green, 1983). Samples with mixed ages, indicated by χ^2 values <5% and large age dispersion values (>20%)

were deconvolved into their principal age components using the binomial peak-fitting method (Table 1). Errors are cited at the 95% confidence level.

Three zircons from the young population of Sanfu sample 42-01 were extracted from the ZFT mount to be dated by the U-Th/He (ZHe) method following the procedures of Reiners (2005). The α-ejection formula used for the He age calculation takes into account the ≤50% reduction of the grain size due to polishing of the fission-track mount.

Zircon U-Pb dating was by LA-ICPMS using a New Wave 213 aperture imaged frequency quintupled laser ablation system (213nm) coupled to an Agilent 750 quadrupole-based ICP–MS. Real time data were processed using GLITTER. Repeated measurements of external zircon standard PLESOVIC (TIMS reference age 337.13±0.37 Ma; Sláma *et al.*, 2008) and NIST 612 silicate glass (Pearce *et al.*, 1997) were used to correct for instrumental mass bias and depth-dependent inter-element fractionation of Pb, Th and U. Data were filtered using standard discordance tests with a 10% cut off. No initial common lead correction is applied. Uncertainty for the measurement is 3-5 % at 2σ.

4. RESULTS

Apatites were not well preserved in most samples and we found only a small numbers of grains in 5 samples. Of these grains many had effectively zero U ppm and/or lots of inclusions making them uncountable. Only in sample HK1 from Hsiulukuan was a statistically significant young Pliocene (4.1 Ma) grain age component determined (Appendix 1.Supplementary data 1). However, because

of the low number of grains (26) successfully counted these preliminary data are not discussed further here but efforts are continuing to obtain more detrital apatite data.

Zircon fission-track age data are reported in Table 1 and ZHe age data in Table 2. The probability for the χ^2 test was effectively zero for all samples indicating significant variance in single grain ages, i.e. mixed age populations (Galbraith & Laslett, 1993).

Deconvolution of the grain ages into grain-age populations was performed using the Binomfit program (Brandon, 1992; Ehlers *et al.*, 2005) based on the binomial peak-fitting algorithm of Galbraith & Green (1990) and Galbraith & Laslett (1993). For each sample the aim was to analyse as many grains as possible to reduce the statistical probability of missing a source fraction with an ideal target of >117 ages (Vermeesch, 2004). In all cases this ideal condition could not be met due to the technical difficulties of finding large numbers of well-etched grains suitable for counting. This inherent problem reflects both the type of zircon (i.e. source rocks) combined with the high wastage of zircon that comes with the need to make multiple grain mounts that were each etched for a different time to ensure grains with track densities (and therefore likely different sources) are represented in the final dataset.

The fission-track grain age distributions of the Shuilien and Shuimuting samples have Middle-to-Late Pliocene depostional ages between 4.1 and 1.8 Ma and are reported in Figure 4. These samples show dominant Mesozoic age components with a statistically smaller number of Palaeozoic and Cenozoic age

components (Table 1, Fig. 4). The youngest grains range between 27.2 and 19.2 Ma with the exception of sample SM1 that has one young grain dated at 7.7 Ma while the rest of the population distribute at ages older than 20 Ma (Table 1, Fig. 4).

The Sanfu and Hsiukuluan samples span the transition from late Pliocene to Pleistocene with depositional ages between 2.58 and 0.78 Ma, and their grain age distributions are reported in Figure 5. These samples have populations older than 6 Ma, similar to those observed at Shuilien and Shuimuting, and all, except two, of them have populations younger than 6 Ma. The Sanfu samples all have grains <6 Ma and their percentage increases upsection. In the oldest samples (40-01) only one grain out of 50 is dated at 5.7 Ma while the rest of the population is older than 18 Ma. Samples 41-01 to 43-01 contain a component <6 Ma that increases from 5% to 38%, and they contain also a component bracketed between 6 and 11 Ma. However, only the two uppermost samples have a well defined young population that in both samples is dated at 2.8 Ma. The Pliocene sample from Hsiukuluan (HK1) contains no age component <6 Ma (Fig. 3) and its youngest grain is 29 Ma but in all the Pleistocene samples at least 60% of the grains are younger than 6 Ma (Table 1; Fig. 3). In the Pleistocene sandstone samples (HK2-4) 71 to 79% of the grains give age populations in the range 3.8 to 4.9 Ma. The cobble sample HK5 of Pleistocene age gives two age populations of 2.6 and 4.4 Ma and the pooled age for the whole sample is 3.5 ± 0.4 Ma (Appendix 1. Supplementary data 2). This suggests that despite its relatively high age dispersion (24.7%), this sample is likely fully reset and its cooling age can be

determined with the zeta method (Hurford & Green, 1983) that gives an age of 3.4 ± 0.5 Ma for 94% of the grains. The fact that there is no significant difference between the pooled age and the zeta age supports the hypothesis that this sample is fully reset.

Three grains from sample 42-01 that have ZFT ages in the range 3.6 to 1.6 Ma (Table 2, Fig. 5) were also dated using the ZHe method. This sample was selected for ZHe dating as it is the oldest sample from the Sanfu section with a well defined and significant Pliocene age population (~2.8 Ma (16%), Table 1). He ages for these three grains are in excellent agreement and range between 2.3 and 3.2 Ma with 1σ values of $\pm$ 0.5 and $\pm$ 0.7 Ma. Two He ages are, as expected, younger than the respective ZFT age, one He age (2.4 ± 0.7 Ma) is older, but still within error of the ZFT age (1.6 -0.2/+5.6 Ma) (Table 2).

Using the double dating technique of Carter & Moss (1999) FT grains from samples SM6 and HK3 were analysed by the U/Pb method. These samples were selected because of the large number of grains of suitable size for LA-ICPMS U-Pb analyses. Grain ages range from 2546 to 22 Ma. Most grains belong to age clusters at 1800- 2000 Ma, 800-1000 Ma, 400-500 Ma, 250-300 Ma 180-220 Ma and 22-30 Ma (Fig. 6; Appendix 1. Supplementary data 3). Of these more than 25% of the grains from Shuimuting, but no grains from Hsiukuluan have the same U-Pb and ZFT age (Fig. 6).

5. PROVENANCE OF DETRITAL ZIRCONS

5.1 THERMOCHRONOMETRIC SIGNATURES OF DETRITAL ZIRCONS

The detrital U/Pb ages range from 22 to 2546 Ma (DR Table 3, Fig. 6) reflecting a variety of possible source areas including the Taiwan orogen, the Luzon volcanic arc and the Eurasian continent. The oldest syn-collisional deposits in the Coastal Range consist of sediments reworked from the Taiwan orogen with a minor component of grains having a magmatic-arc provenance (Dorsey, 1988; 1992). Modern Taiwan consists largely of Neogene sandstones and mudstones that were derived from the Eurasian continent, deposited in the China Sea, and later incorporated in the orogen. One parameter that can be used to distinguish between continent-derived or arc-derived versus modern reset Taiwan-derived zircons is the zircon FT grain age.

The high-grade metamorphic rocks exposed in modern Taiwan have ZFT ages in the 6-1 Ma range (Fig. 2), thus recent Taiwan-derived fully-annealed zircons should be younger than or equal to 6 Ma (≤6 Ma). Zircons derived from the Luzon volcanic arc should be Miocene (16 - 6 Ma) (Huang *et al.*, 2006), and older zircon fission-track ages should represent non-reset detrital cover material in the Taiwan orogen and material originally derived from the Eurasian continent.

Evidence of the original sedimentary cover is retained in the Hsuehshan Range and in the Backbone Slates where detrital ZFT ages range from the Oligocene to Carboniferous whereas thermally reset ZFT samples yield grain ages from 1 to 9 Ma (Liu, 1988; Liu *et al.*, 2001) (Fig. 2).

Zircon (U-Th)/He ages from the Hsuehshan Range and Backbone Slates give results similar to the fission-track ages, with reset ages from the more deeply exhumed parts of the Backbone Slates and Hsuehshan Range ranging

from 0.5 Ma to 4.3 Ma and ages from less exhumed regions being over 10 Ma (Beyssac *et al.*, 2007).

The older age components measured during this study are similar to the unreset grain ages described for the Hsuehshan Range which are considered to be sourced from Mesozoic and pre-Mesozoic granitic rocks in southeastern China (Liu, 1988; Liu *et al.,* 2001). The U-Pb data yielded age components at 1800-2000 Ma, 800-1000 Ma, 400-500 Ma, 250-300 Ma and 180-220 Ma consistent with an original source in continental southeast China. The key tectonothermal events that have affected south China are summarized in Table 3. The Luliangian (>1500 Ma) zircon U-Pb age grains from sample SM6 have had their fission-tracks reset most recently by the Mesozoic Yenshanian event (Fig. 6). The fission-track and U-Pb ages from other grains cluster around significant crust building events (Fig. 6). This suggests that the bulk of the fission-track ages record exhumational cooling from these tectonothermal events such that the southeast China source signal has been preserved.

The youngest grains from sample SM6 yield concordant U-Pb and fission-track grain ages from 22.7±1.7 to 31.5±3.2 Ma, indicating magmatic crystallisation of this age (Fig. 6). Volcanic detritus also forms a major component in samples from the Fanshuliao Formation of the Coastal Range (Dorsey, 1988). Potential magmatic sources include the Luzon volcanic arc to the east and intra-plate volcanism that is presently exposed to the north and west in northern Taiwan. Pooled zircon fission-track ages from the Chimei igneous complex (23° 30’ S), which represents the northern accreted parts of the Luzon arc, range from

13.0±1.0 to 15.6±1.1 Ma (Yang *et al.,* 1988). Similar Mid Miocene eruption ages are recorded for the Penghu volcanic islands (16.2–8.2 Ma; Juang & Chen, 1992) to the west (Fig. 1). Neogene volcanism in the form of lava flows, dykes and sills preserved in sediments is recorded in northern Taiwan. The volcanism in that area has been dated as Late Oligocene/Early Miocene (~ 23 ± 2 Ma) using the fission-track method (Chen *et al.,* 2001).

Shuimuting sample SM1 is notable in that it comes from the Fanshuliao Formation, which is thought to have a major volcanic component (e.g. Dorsey, 1988), and has a single grain dated at 7.6 Ma (Table 1). However, sample SM6 contains no middle Miocene U-Pb ages (~16 to 11 Ma) similar to those measured from the Luzon volcanic arc in this region (Yang *et al.,* 1988). This suggests that some or most of the volcaniclastic sediment of the Fanshuliao Formation may not be sourced directly from rocks of the Luzon volcanic arc, as proposed by previous workers (Chi *et al.*, 1981; Dorsey, 1988; Dorsey & Lundberg, 1988), but instead from northern Taiwan. This is consistent with the abrupt change in sediment composition and provenance at the base of the Pliocene section (Dorsey, 1988). A source to the north is also consistent with available palaeocurrent data which shows overall transport to the south as recorded in the Pliocene sediments (Chen & Wang, 1988; Dorsey & Lundberg, 1988) (Fig. 1).

Three more samples from Sanfu show late Miocene ZFT age components that could be related to arc-volcanism, but no U-Pb data are available for these grains. Nevertheless, it is important to note that the Sanfu samples show a rejuvenating trend of detrital ages, and this trend precedes by ~0.4 Ma the

appearance at Hsiukuluan of large grain age fractions (at least 60%) younger than 6 Ma. The Pleistocene Hsiukuluan sediments represent a submarine fan system sourced from metamorphic rocks to the west and the sediments sampled at Sanfu are the first interval of coarse, quartz-rich turbidites. These observations suggest that the Hsiukuluan and Sanfu sediments are likely parts of the same clastic wedge that evolved through time and space recording the unroofing of the metamorphic rocks of Taiwan. In this framework, the late Miocene zircon grains may be sourced from reset or partially reset metamorphic rocks of proto-Taiwan rather than the volcanic arc.

5.2. SEDIMENT ROUTING OF DETRITAL ZIRCONS

Conditions for Plio-Pleistocene sediment dispersal are considered to have been different than today, as the present-day Longitudinal Valley did not exist to channel sediment axially from the Central Range. Furthermore, the position of the topographic divide in the Taiwan orogen may have migrated eastwards through time. This is predicted by the development of a steady-state topography in Taiwan (Willett *et al.*, 2003; Fuller *et al.*, 2006), and suggests that the Pliocene to early Pleistocene sediment source area feeding the collisional basin may have extended further west than today.

Available palaeocurrent data suggest that during early to middle Pliocene time, currents transporting the sediment were highly variable but with a dominant signal from the north-northwest parallel to the modern coast (Chen & Wang, 1988; Dorsey & Lundberg, 1988) (Fig. 1). The region around Hsiukuluan is an

exception as the palaeocurrents all record transport to the east, away from the evolving orogen (Fig. 1). Basin geometry, slope instability and local drainage clearly affect sediment dispersal as is evident off SE Taiwan today (Malavieille & Trullenque, 2009). Similar controls may have affected sediment transport during the early stages of the development of the retro-foredeep. In the late Miocene – early Pliocene the submarine palaeotopography was associated with the subsiding volcanic arc, which consisted of discrete volcanic centres and fringing reefs. These features potentially channelled sediment into distinct deep-sea submarine-fan environments (Chen & Wang, 1988). After this early stage the basin evolved to form a south dipping tempestite-turbidite ramp (Dorsey & Lundberg, 1988) which is consistent with the available Pliocene palaeoflow data.

Despite the effects of the basin paleotopography and of the dynamics of sediment accumulation, our data consistently indicate that during the early-middle Pliocene no Taiwan-derived reset zircons reached the retro-foredeep and that only in the very late Pliocene reset zircons were deposited in the Hsiukuluan-Sanfu fan-system that was fed from the west.

6. LAG TIMES AND EXHUMATION RATES

Our zircon fission-track data record a clear unroofing sequence of the metamorphic rocks of Taiwan. This sequence is shown by the stratigraphic younging of the detrital zircon age components and by the increase in zircons with young reset ages in the early Pleistocene (Fig. 5; 7). The younging trend is interpreted as representing the removal of rock overburden bearing unreset

zircon followed by exposure and erosion of rocks with reset zircon fission-track ages (Fig. 7). The closure temperature T_c of the ZFT system is ~ 240°C (Brandon *et al.*, 1998) indicating that the exposure of reset zircon fission-track ages occurs after removal of a rock column of 3-9 km thickness according to thermal structure of the shallow crust. Our data indicate that the removal of this cover occurred between ~4 and 1.9 Ma, and therefore they indicate that the source area of the syncollisional sediments was rapidly exhuming and eroding during this time. This is consistent with the unroofing trend that was previously documented using sandstone petrography in the Coastal Range (Dorsey, 1988).

The young detrital age components with a reset modern Taiwan-provenance signature (<6 Ma) can be used to calculate exhumation rates through the application of the 'lag time' concept (Garver *et al.*, 1999). The lag time is the time taken for a sample to be exhumed from the depth of closure of the thermochronometer to the surface and then deposited in a nearby, genetically related basin. Assuming transport times are negligible, the lag time provides an estimate of the cooling time which can be converted to an exhumation rate.

The young population ages of the Pleistocene Hsiukuluan samples range from 2.6 to 4.9 Ma, yielding lag times of between 1 and 4 million years. These "paleo-cooling ages" are in the same range as the modern cooling ages of Taiwan (Fig. 2). The resulting exhumation rates assuming steady-state are ~2-7 km/Myr, using a surface temperature of 10°C and a geothermal gradient of 25°C/km for the Central Range. Correcting for advection of isotherms by one-

dimensional heat conduction using the approach of Reiners & Brandon (2006) we calculate exhumation rates of 1.6-2.5 km/Myr.

The (U-Th)/He-dated zircons from the Sanfu section provide a more accurate lag time that potentially better reflects late Pliocene cooling of the Taiwan metamorphic rocks. The stratigraphic age is 1.88 $\pm$ 0.07 Ma, ZHe cooling ages are 3.2 - 2.3 Ma and the resulting lag times range between 0.4 and 1.3 million years. Following Reiners & Brandon (2006), assuming thermal steady-state and an initial geothermal gradient of 25°C/km, the estimated exhumation rates are between 2 and 4 km/Myr. This is resolved over a time window that initiated between 3.2 Ma and 2.3 Ma (ZHe age of grains) and ended at the deposition age of 1.9 Ma (Fig. 5). If no thermal steady-state is assumed, the resulting exhumation rates are much higher in the range 3-10 km/Myr. This suggests that exhumation rates of 2-4 km/Myr might be underestimated if during the late Pliocene the sub-aerial exposure of the wedge was still in an initial stage and erosion had not been sufficient for the orogen to reach an exhumational steady-state.

The estimated late Pliocene exhumation rates of ≥2-4 km/Myr from ZHe dating individual grains are similar to the long-term exhumation rates based on cooling ages of the present basement that shows average rates between 4 and 6 mm/yr (Liu *et al.*, 2000; Willett *et al.*, 2003). This result is similar also to the exhumation rate of 4 – 5 km/Myr that was based on qualitative analysis of metamorphic lithic fragments in Coastal Range sandstones (Dorsey, 1988). The

combined results of this and previous studies confirm that the modern high exhumation rates of Taiwan have been sustained since late Pliocene time.

7. ONSET OF HIGH EXHUMATION RATES AND TECTONIC EVOLUTION

As discussed in section 2.2, data from the foredeep basins (Chi *et al.*, 1981, Dorsey *et al.* 1988, Lin *et al.*, 2003), cooling ages from the basement (Liu *et al.* 2001, Willett *et al.*, 2003, Beyssac *et al.*, 2007) and geodynamic reconstructions (Suppe, 1984) indicate that arc-continent collision occurred during the late Miocene-early Pliocene between ~6.5 and 4 Ma (Chi *et al.*, 1981, Dorsey *et al.* 1988, Lin *et al.*, 2003). Based on lag times, it is possible to derive how long it took since arc-continent collision to expose reset ZFT ages during the Pliocene. To this aim, it is necessary to calculate the closure depth for the ZFT system, which at high exhumation rates is significantly affected by heat advection that causes upwarping of the isotherms. We can account for the effect of advection with the same method used to derive exhumation rates from lag times (Reiners & Brandon, 2006). For exhumation rates of ≥2-4 km/Myr the ZFT closure depth is predicted to be ≤ 3.5 km. Thus, even at the lowest exhumation rates the exposure of reset ZFT would take ~2 Myr. If arc-continent collision occurred in the late Miocene (~6.5 Ma, Lin *et al.*, 2003), and if exhumation rates of ≥2-4 km/Myr were sustained since collision, then reset ZFT ages would be evident in Pliocene sediments deposited between ~ 5 and 4 Ma. This is at odds with our data showing that reset ZFT and ZHe ages are present in sediments that were deposited since 1.9 Ma. Thus, if arc-continent collision occurred in the late

Miocene (~6.5 Ma, Lin *et al.*, 2003), exhumation rates must have been low from ~6.5 to 5 and must have increased to ≥2-4 km/Myr between 5 and 3 Ma. Alternatively, if exhumation rates of ≥2-4 km/Myr have remained constant since arc-continent collision, then collision must have occurred during the early-middle Pliocene.

Despite the uncertainties on the timing of arc-continent collision, a wealth of data indicates that at 5-3 Ma major changes occurred in the Taiwan orogen. At the local scale, the retro-foredeep records an increase of both the grain-size of the syn-collisional sediments and the sediment accumulation rates from ca. 0.5mm/yr at 3-4 Ma to ~3.6mm/yr between 2 and 1 Ma (Chi *et al.*, 1981; Dorsey & Lundberg, 1988). Although these modifications could reflect simply local sedimentary processes, also regional scale changes are recorded during this time. In the retro-foredeep accelerated subsidence of the collapsing arc at ~3 Ma resulted in an increase of the accommodation space (Dorsey & Lundberg, 1988; Dorsey, 1992). An acceleration in subsidence is recorded starting from 4 Ma in the foreland basin (Lin, 2003, Lee *et al.*, 2006). Thermokinematic models of the Central Range indicate that the wedge kinematics might have switched from frontal accretion to underplating at 4 Ma (Beyssac *et al.*, 2007). Thus, during the late Pliocene-early Pleistocene major local and regional modifications occurred and the observed processes provide evidence in support of thickening of the orogenic wedge, underplating and growth of topography (Fuller *et al.*, 2006). The overall effect of these processes was likely an increase of the eroded surface area and of the relief, that may have resulted in an increase of sediment grain-

size, sediment yield and exhumation rate. The time lag between the onset of arc-continent collision at 6.5 Ma and the acceleration of subsidence in the foredeep basins, the thickening of the wedge by underplating and the growth of topography could reflect simply the response time of the orogenic wedge to adjust to the destabilising effect of collision.

In this model, collision occurred during the late Miocene - early Pliocene and at this time the source area of the studied sedimentary succession was similar to the modern Hengchun Peninsula. The Hengchun region is a domain of incipient continental subduction which forms the recently emerged portion of the orogenic wedge and is characterized by a subdued topography, low exhumation rates and the exposure of only partially reset zircons (time period A; Fig. 8). In the Hengchun Peninsula north of ~22°N, slope sediments from the continental margin are involved in the accretionary wedge and are deformed and metamorphosed (Malavieille & Trullenque, 2009). As predicted by Coulomb wedge theory (Davis *et al*., 1983), an increase of the flux of accreted material would destabilise the wedge because the influx must be balanced by the efflux in order to maintain exhumational steady state. Thus, in our model the increase in exhumation rates observed from about 5-3 Ma can be related to the increase of influx that occurred during incipient arc-continent collision as the sediments from the continental margin were involved in the accretionary wedge. Finally, this increase in exhumation has resulted in the exposure of reset zircon grains in the late Pliocene and in the large zone of reset zircon fission-tracks observed today (Fig. 8).

8. CONCLUSIONS

Dating of detrital zircons derived the Plio-Pleistocene Taiwan orogenic belt has resolved an increase of exhumation rate between 5 and 3 Ma. Zircon fission-track grain ages from ~2 - 4 million year old sediments yield early Tertiary or Mesozoic fission-track ages, indicating that they were not thermally reset by late Tertiary thermal events related to the Taiwan Penglai orogen. The age distribution in these samples is similar to that of sediments sourced from south-eastern China (Liu, 1988; Liu *et al.,* 2001). This is further supported by U/Pb dating of zircons which yielded crystallization ages from the Miocene to the Proterozoic with clusters at times of major Asian orogeny (Fig. 6). The detrital ages in the ~2 - 4 million year old syn-collisional sediments reflect the early stage removal of the sedimentary cover (Fig. 7). Samples with Miocene grain age components potentially record some thermal resetting of zircon during the early stages of collision.

In contrast, sediments younger than 1.9 Ma yield zircons with fission-track ages as young as Pliocene (Fig. 7). Lag times from these fission-track ages and from more accurate (U-Th)/He ages suggest exhumational cooling, transport and deposition occurred within 1- 4 Myr, similar to modern exhumation rates. Double-dating by fission-track and (U-Th)/He methods was particularly effective at resolving this short lag age. A rapid change in lag age which reflects a very short transition from slow surface uplift and erosion to rapid exhumation occurred at the same time as major changes in the wedge dynamics including an increase in

subsidence rate in the foredeep basins and the onset of underplating (Dorsey & Lundberg, 1988; Beyssac *et al.*, 2007). We estimate that the transition to rapid exhumation started between 3 and 5 Myr, and that the high exhumation rates have continued at approximately the same rate until the present day.

ACKNOWLEDGEMENTS

This work was supported by NERC grant NE/E012426/1 and a Royal Society of Edinburgh-Scottish Executive fellowship to Kirstein, and by a post-doctoral and Marco Polo fellowship from the University of Bologna to Fellin. This work was supported in part by US National Science Foundation grant EAR 0337782.

REFERENCES

BEYSSAC, O., SIMOES, M., AVOUAC, J.P., FARLEY, K.A., CHEN, Y.G., CHAN, Y.C. & GOFFE, B. (2007) Late Cenozoic metamorphic evolution and exhumation of Taiwan. *Tectonics* **26**, TC6001, doi:10.1029/2006TC002064.

BRANDON, M.T. (1992) Decomposition of fission-track grain-age distributions. *Am. J. Sci.* **292**, 535-564.

BRANDON, M.T., RODEN-TICE, M.K. & GARVER, J.I. (1998) Late Cenozoic exhumation of the Cascadia accretionary wedge in the Olympic Mountains, northwest Washington State. *Geol. Soc. Am. Bull.* **110**, 985-1009.

BYRNE, T. & LIU, C.S. (2002) Preface: Introduction to the geology and geophysics of Taiwan. In: *Geology and Geophysics of an Arc-Continent Collision, Taiwan* (Ed. by T. Byrne & C.S. Liu) Special Paper Boulder, Geological Society of America. **358**, v-viii.

CARTER, A. & MOSS, S.J. (1999) Combined detrital-zircon fission-track and U-Pb dating: A new approach to understanding hinterland evolution. *Geology* **27**, 235-238.

CHANG, C.-P., ANGELIER, J., LEE, T.-Q., HUANG, C.-Y. (2003) From continental margin extension to collision orogen: structural development and tectonic

rotation of the Hengchun peninsula, southern Taiwan. *Tectonophysics* **361**, 61–82.

CHEN, C.H., CHUNG, S.-H., HWANG, H.-H., CHEN, C.-H. & CHUNG, S.-L. (2001) Petrology and Geochemistry of Neogene Continental Basalts and Related Rocks in Northern Taiwan(III): Alkali Basalts and Tholeiites from Shiting-Yinko Area *West. Pac. Earth Sci.* **19**, 19-46.

CHEN, W.-S. & WANG, Y. (1988) Development of deep sea fan systems in Coastal Range basin, eastern Taiwan. *Acta Geol. Taiwan*. **26**, 37-56.

CHI W.R., NAMSON J. & SUPPE J. (1981) Stratigraphic record of plate interactions in the Coastal Range of eastern Taiwan. *Geol. Soc. China Memoir* **4**, 155–194.

DADSON S.J., HOVIUS N., CHEN H., DADE B. W., HSIEH M.-L., WILLETT S.D., HU J.-C., HORNG M.-J., CHEN M.-C., STARK C.P., LAGUE D. & LIN J.-C. (2003) Links between erosion, runoff variability and seismicity in the Taiwan orogen. *Nature*, **426**, 648-651.

DADSON, S. J., HOVIUS, N., CHEN, H., DADE, B., LIN, J.C., HSU, M.L., LIN, C.W., HORNG, M.J., CHEN, T.C., MILLIMAN, J. & STARK, C.P. (2004). Earthquake-triggered increase in sediment delivery from an active mountain belt. *Geology* **32**, 733-736.

DORSEY, R.J. (1988) Provenance evolution and unroofing history of a modern arc-continent collision: Evidence from petrography of Plio-Pleistocene sandstones, eastern Taiwan. *J. Sediment. Petrol*. **58**, 208-218.

DORSEY, R.J. (1992) Collapse of the Luzon volcanic arc during onset of arc-continent collision: Evidence from a Mio-Pliocene unconformity, eastern Taiwan. *Tectonics* **11**, 177-191.

DORSEY, R.J., BUCHOVECKY, E.J. & LUNDBERG, N. (1988) Clay mineralogy of Pliocene-Pleistocene mudstones, eastern Taiwan: Combined effects of burial diagenesis and provenance unroofing. *Geology,* **16**, 944-947.

DORSEY, R.J. & LUNDBERG, N. (1988) Lithofacies analysis and basin reconstruction of the Plio-Pleistocene collisional basin, Coastal Range of eastern Taiwan. *Acta Geol. Taiwan*. **26**, 57-132.

EHLERS T. A., CHAUDHRI T., KUMAR S., FULLER C. W., WILLETT S. D., KETCHAM R. A., BRANDON M. T., BELTON D. X., KOHN B. P., GLEADOW A. J. W., DUNAI T. J., FU F. Q. (2005) Computational tools for low-temperature thermochronometer interpretation. *Reviews in Mineralogy and Geochemistry,* **58**, 589-622.

ERNST W. G., JAHN, B. M. (1987) Crustal accretion and metamorphism in Taiwan, a post-Palaeozoic mobile belt. *Philosophical Transactions of the Royal Society of London,* **A321**, 129-161.

FISHER D. M., WILLETT, S., EN-CHAO, Y., CLARK, M.B. (2007) Cleavage fronts and fans as reflections of orogen stress and kinematics Taiwan. Geology 35, 65-68.

FULLER, C.W., WILLETT, S.D., FISHER, D. & LU, C.Y. (2006) A thermomechanical wedge model of Taiwan constrained by fission-track thermochronometry: *Tectonophysics*, **425**, 1-24.

GALBRAITH, R.F. & GREEN, P.F. (1990) Estimating the component ages in a finite mixture. *Nucl. Tracks Rad. Measure*. **17**, 197-206.

GALBRAITH, R.F. & LASLETT, G.M. (1993) Statistical models for mixed fission-track ages. *Nucl. Tracks Rad. Measure*. **21**, 459-470.

GARVER, J.I., BRANDON, M.T., RODEN-TICE, M. & KAMP, P.J.J. (1999) Exhumation history of the orogenic highlands determined by detrital fission-track thermochcronology. In: Exhumation Processes: Normal faulting, ductile flow and erosion. Ed. by Ring, U., Brandon, M.T., Lister, G.S. & Willett, S.D. *Geol. Soc. Lond. Spec. Pub.* **154**, 283-304.

GRADSTEIN F., OGG, J., SMITH, A. (2004) A Geologic Time Scale. 589 pp. Cambridge University Press.

HO C-S. (1999) An introduction to the geology of Taiwan. 192 pp. Central Geological Survey, Taiwan, ROC.

HORNG C.-S., SHEA K.-S. & LEE J.-C. (1999) Magnetobiostratigraphy of the Sanfu-chi section in the Coastal Range of Eastern Taiwan: new results. *J. Geol. Soc. China.* **42**, 613-629.

HUANG C.-Y., YUAN P. B. & TSAO S.-J. (2006) Temporal and spatial records of active arc-continent collision in Taiwan: A synthesis. *GSA Bulletin*, **118**, 274–288.

HURFORD, A.J. & GREEN, P.F. (1983) The zeta calibration of fission-track dating. *Iso. Geosci.* **1**, 285-317.

JUANG, W. S. & CHEN, J.C. (1992). Geochronology and geochemistry of Penghu basalts, Taiwan Strait and their tectonic significance. *Southeast Asian Earth Sci.* **7**, 185-193.

LEE, T.Q., KISSEL, C., BARRIER, E., LAJ, C. & CHI, W.R. (1991) Palaeomagnetic evidence for a diachronic clockwise rotation of the Coastal Ranges, eastern Taiwan. *Earth Planet. Sci. Lett*. **104**, 245-257.

LEE, Y.-H., CHEN, C.-C., LIU, T.-K., HO, H.-C., LU, H.-Y. & LO, W. (2006) Mountain building mechanisms in the Southern Central Range of the Taiwan Orogenic Belt — From accretionary wedge deformation to arc–continental collision. *Earth Planet. Sci. Lett.* **252**, 413-422.

LI, Y.-H. (1976). Denudation of Taiwan Island since the Pliocene Epoch. *Geology* **4**, 105-107.

LIN A. T., WATTS, A.B., HESSELBO, SP. (2003) Cenozoic stratigraphy and subsidence history of the South China Sea margin in the Taiwan region. *Basin Research,* **15**, 453-478.

LIU, T.K. (1988) Fission-track dating of the Hsueshan Range: thermal record due to arc-continent collision in Taiwan. *Acta Geol. Taiwan*. **26**, 279-290.

LIU, T.-K., CHEN, Y.-G., CHEN, W.-S. & JIANG, S.-H. (2000) Rates of cooling and denudation of the Early Penglai orogeny, Taiwan, as assessed by fission-track constraints. *Tectonophysics* **320**, 69-82.

LIU, T.-K., HSIEH, S., CHEN, Y.-G. & CHEN, W.-S. (2001) Thermo-kinematic evolution of the Taiwan oblique-collision mountain belt as revealed by zircon fission-track dating. *Earth Planet. Sci. Lett*. **186**, 45-56.

LO C.-H. & ONSTOTT T.C. (1995) Rejuvination of K-Ar systems in the Taiwan Mountain Belt, *Earth Planet. Sci. Lett*. **131**, 7-98.

LU C.-Y. & HSÜ K.J. (1992) Geology of the Taiwan mountain belt. *Petr. Geol Taiwan*. **27**, 21-46.

LUNDBERG N. & DORSEY R. J. (1990) Rapid Quaternary emergence, uplift, and denudation of the Coastal Range, eastern Taiwan. *Geology* **18**(7), 638-641.

MALAVIEILLE, J. & TRULLENQUE, G. (2009) Consequences of continental subduction on forearc basin and accretionary wedge deformation in SE Taiwan: Insights from analogue modelling. *Tectonophysics*, **466**, 377-394.

PEARCE, N.J.G, PERKINS, W.T., WESTGATE, J.A., GORTON, M.P., JACKSON, S.E., NEAL, C.R. & CHENERY, S.P. (1997) A compilation of new and published major and trace element data for NIST SRM 610 and NIST SRM 612 glass reference materials. *Geostandards News*. **21**,115-144.

RAHL J., EHLERS, T.A., VAN DER PLUIJM, B.A. (2007) Quantifying transient erosion of orogens with detrital thermochronology from syntectonic basin deposits. *Earth and Planetary Science Letters,* **256**, 147–161.

REINERS, P.W. (2005) Zircon (U-Th)/He Thermochronometry. In: Low temperature thermochronology. Ed. by P.W. Reiners & T.A. Ehlers, *Reviews Mineral. Geochem*. **58**, 151-176.

REINERS, P.W. & BRANDON, M.T. (2006) Using thermochronology to understand orogenic erosion, *Annual Rev.Earth Planet. Sci*. **34**, 419-466.

SCHALLER, M., HOVIUS, N., WILLETT, S.D., IVY-OCHS, S., SYNAL, H.-A. & CHEN, M.-C. (2005) Fluvial bedrock incision in the active mountain belt of Taiwan from in situ-produced cosmogenic nuclides. *Earth Surf. Proc. Land*. **30**, 955-971.

SHYU, J. B. H., SIEH, K., AVOUAC, J-P., CHEN, W.S. & CHEN, Y.G. (2006). Millennial slip rate of the Longitudinal Valley fault from river terraces: Implications for convergence across the active suture of eastern Taiwan. *J. Geophysic. Res.* **111**, B08403.

SIBUET J.-C., HSU S.-K., LE PICHON X., LE FORMAL J.-P., REED D., MOORE G. & LIU C.-S. (2002) East-Asia plate tectonics since 15 Ma: constraints from the Taiwan region. *Tectonophysics* **344**, 103-134.

SIBUET J.-C., HSU S.-K. & DEBAYLE E. (2005) Geodynamic context of the Taiwan Orogen, In: Continent-ocean interactions within East Asian marginal seas. Ed. by P. Clift, W. Kuhnt, P. Wang & D. Hayes *Geophysical Monograph* **149**, 127-158.

SIMOES, M., AVOUAC, J.P., BEYSSAC, O., GOFFE, B., FARLEY, K.A. & CHEN, Y.-G. (2007). Mountain-building in Taiwan: a thermo-kinematic model. *Jour. Geophys. Res.* **112**, B11405.

SLÁMA, J., KOSLER, J., CONDON, D.J., CROWLEY, J.L., GERDES, A., HANCHAR, J.M., HORSTWOOD, M.S.A., MORRIS, G.A., NASDALA, L., NORBERG, N., SCHALTEGGER, U., SCHOENE, B., TUBRETT, M.N. & WHITEHOUSE, M.J. (2008) Plesovice zircon - A new natural reference material for U-Pb and Hf isotopic microanalysis. *Chem. Geol.* **249**, 1-35.

SUPPE, J. (1980a) Imbricated structure of western foothills belt, South Central Taiwan. *Petrol. Geol. Taiwan*, **17**, 1–16.

SUPPE, J. (1980b) A retrodeformable cross section of northern Taiwan. *Geol. Soc. China Proc.*, **23**, 46–55.

SUPPE J. (1981) Mechanics of mountain building and metamorphism in Taiwan. *Memoir of the Geological Society of China*, **4**, 67-89.

SUPPE, J. (1984) Kinematics of arc-continent collision, flipping of subduction, and back-arc spreading near Taiwan, *Geol. Soc. China* **6**, 21-34.

TENG, L.S. (1987) Stratigraphic records of the late Cenozoic Penglai orogeny of Taiwan. *Acta Geol. Taiwan*. **25**, 205-224.

TENG, L.S. (1990) Geotectonic evolution of late Cenozoic arc-continent collision in Taiwan. *Tectonophysics* **183**, 57-76.

VERMEESCH, P. (2004) How many grains are needed for a provenance study? *Earth Planet. Sci. Lett.* **224**, 441-451.

WANG P. L., LIN, L. H., LO, C.H. (1998) 40Ar/39Ardating of mylonitization in the Tananao schist, eastern Taiwan. *Journal of the Geological Society China,* **41**, 159 – 183.

WILLETT, S.D., FISHER, D., FULLER, C., EN-CHAO, Y. & CHIA-YU, L. (2003) Erosion rates and orogenic-wedge kinematics in Taiwan inferred from fission-track thermochronometry. *Geology* **31**, 945-948.

YANG, T.-S., LIU, T-K. & CHEN, C-H. (1988) Thermal event records of the Chimei igneous complex: constraint on the ages of magma activities and the structural implication based on fission-track dating. *Acta Geol. Taiwan*. **26**, 237-246.

YEN, J-Y. (2003) Provenance of Miocene sedimentary sequences in the Hengchun Peninsula, southern Taiwan and implications for the modern Taiwan orogen. PhD thesis, *Florida State University*, 133 pgs.

Figures

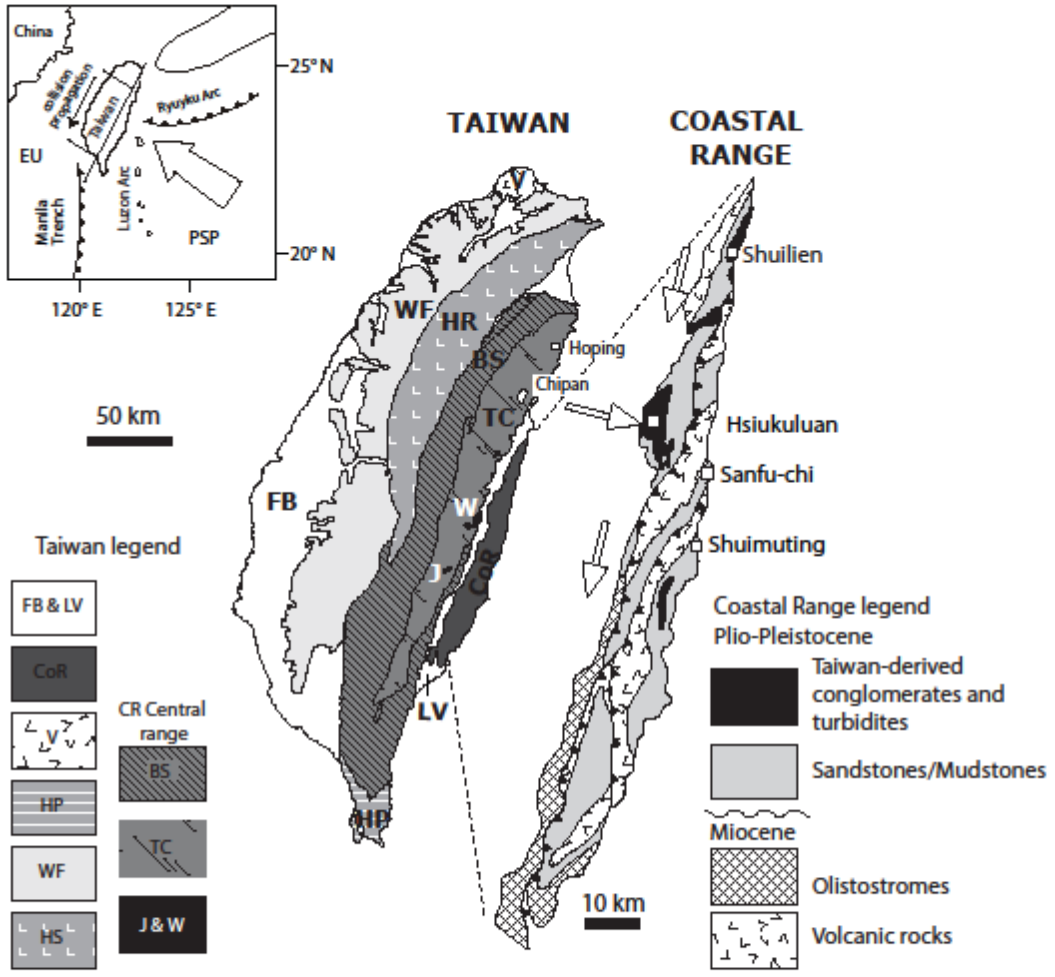

Figure 1. Tectonostratigraphic divisions of Taiwan from west to east include the Coastal Plain (CP), the Western Foothills (WF), the Central Range (HS, BS & TC), the Longitudinal Valley (LV) and the Coastal Range (CoR). Hengchun Peninsula (HP), volcanic rocks in the north-west (V), Ho – Hoping, Ch – Chipan. Inset illustrates the position of Taiwan relative to the China mainland and the main arc-trench systems in the region. Coastal Range geologic map modified after Dorsey & Lundberg (1988). Direction of plate motion after Sibuet *et al.* (2005). Large arrows indicate Pliocene-Pleistocene palaeocurrent directions after Chen & Wang (1988) and Dorsey & Lundberg (1988).

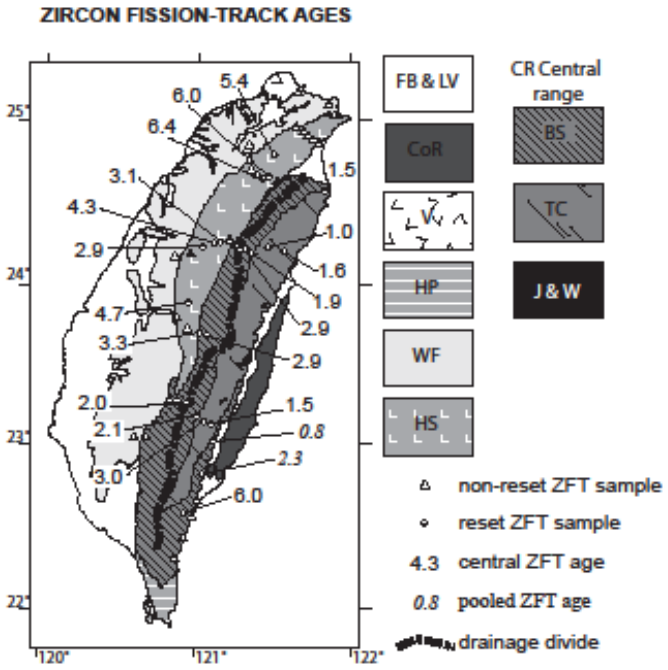

Figure 2. Generalized geological map of Taiwan with zircon fission-track ages from Liu *et al.* (2001) and Willett *et al*. (2003). Legend as in Figure 1. All ages are in millions of years and are central ages except for those in italics which are pooled ages.

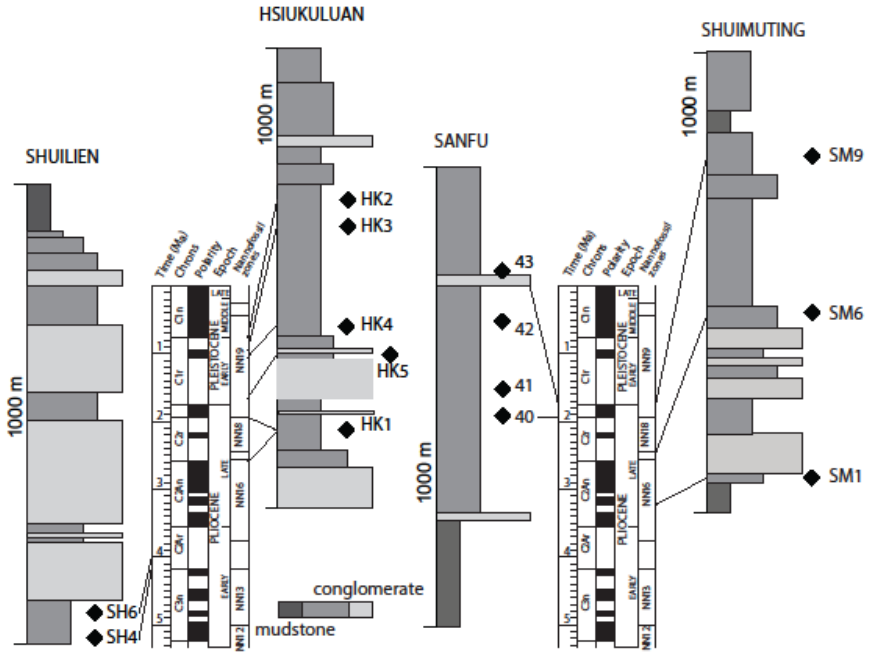

Figure 3. Schematic stratigraphy of sections sampled from Shuilien in the north to Shuimuting in the south. Black diamonds indicate position of samples dated during this study. Depositional ages from Lee *et al*. (1991), Horng *et al.* (1999) corrected to timescale of Gradstein *et al.* (2004).

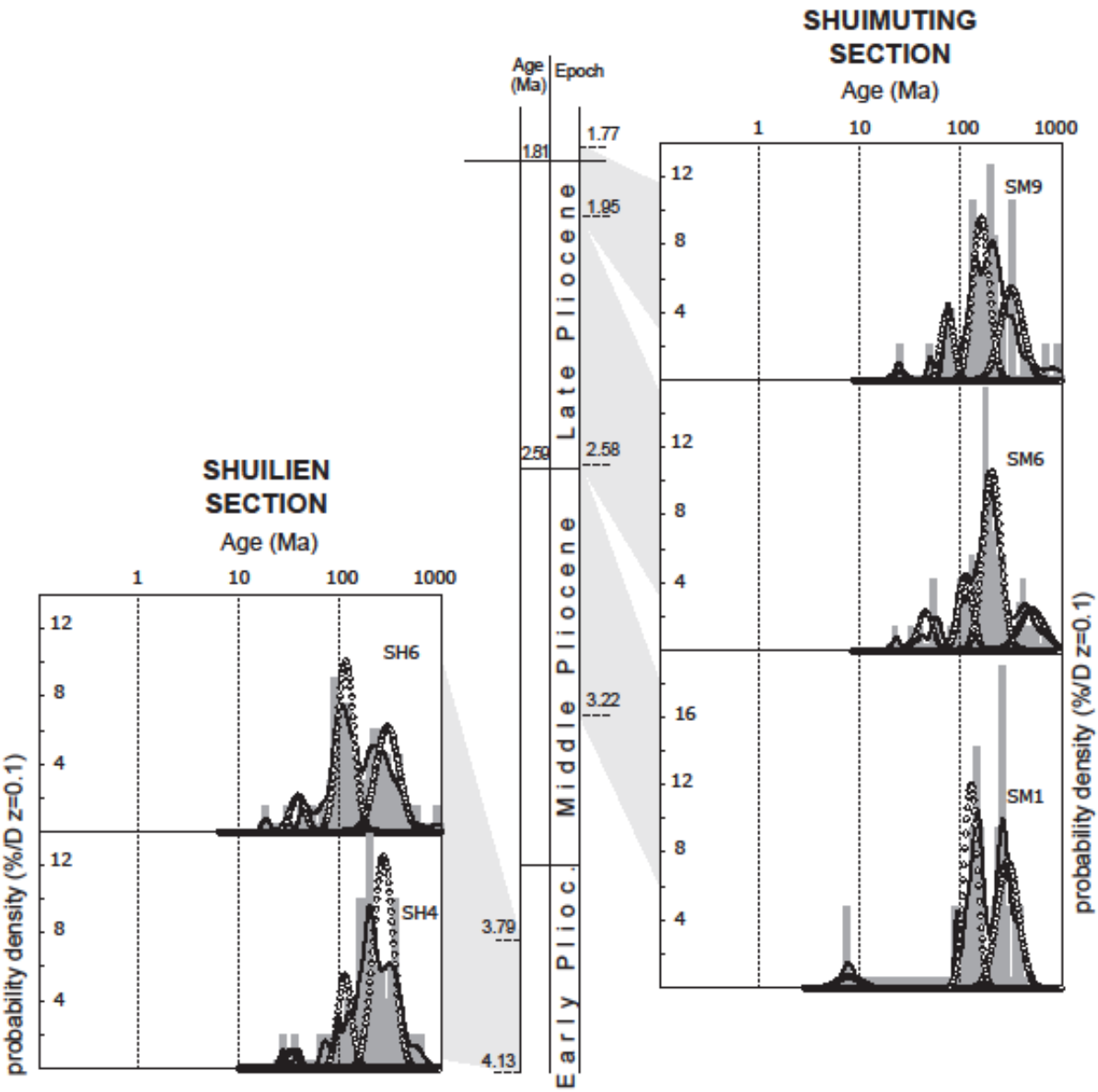

Figure 4. Zircon fission-track grain age distributions for measured samples from the Shuilien and Shuimuting sections highlighting the dominant Mesozoic and Palaeozoic peak age components in Pliocene age sediments. Depositional ages from Lee *et al*. (1991) and C.S. Horng (pers. comm.).

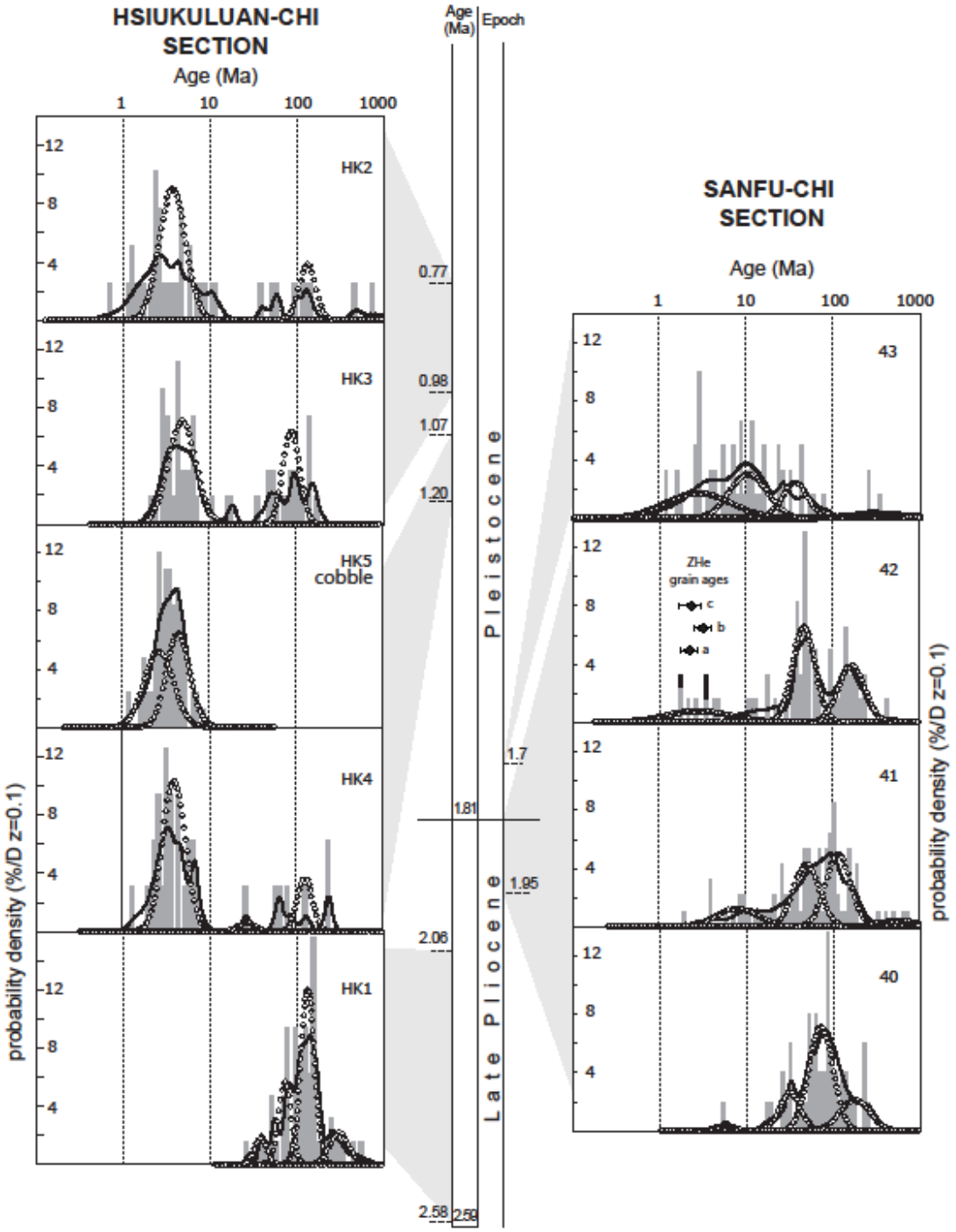

Figure 5. Zircon fission-track grain age distributions for measured samples from the Hsiukuluan and Sanfu sections highlighting significant late Neogene peaks in late Pliocene and Pleistocene time. Grain age peaks discussed in text indicated by white circles. Depositional ages from Lee *et al.*, 1991 and Horng *et al.*, 1999. Darker columns in sample 42 from Sanfu indicate grains double dated by ZHe technique.

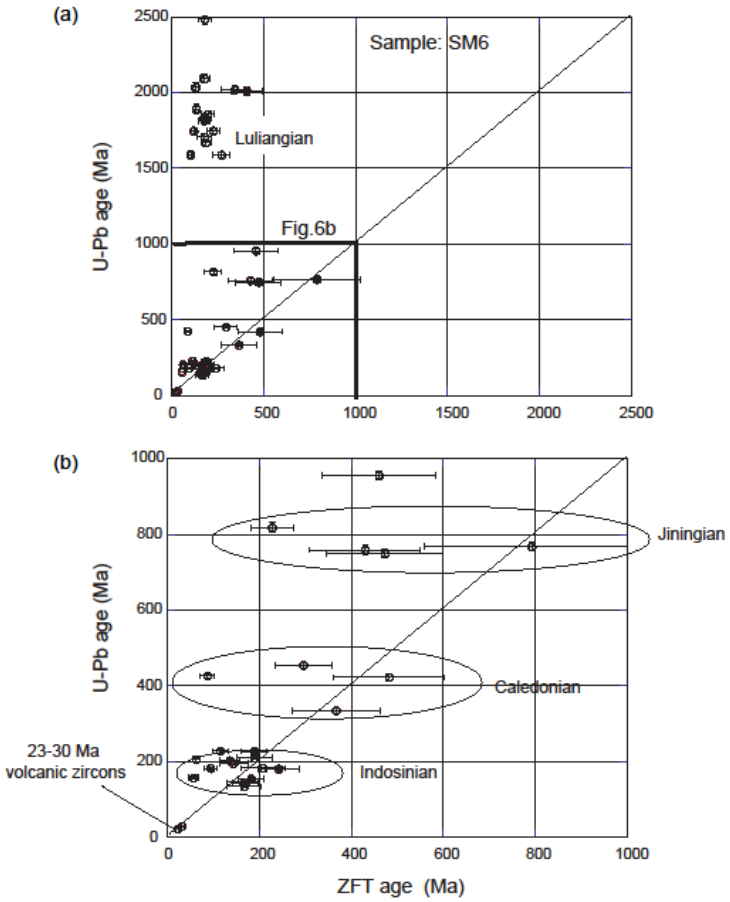

Figure 6. (a) U/Pb versus fission-track ages of sample SM6 from Shuimuting. (b) Ages cluster around significant tectonic events that affected south east China.

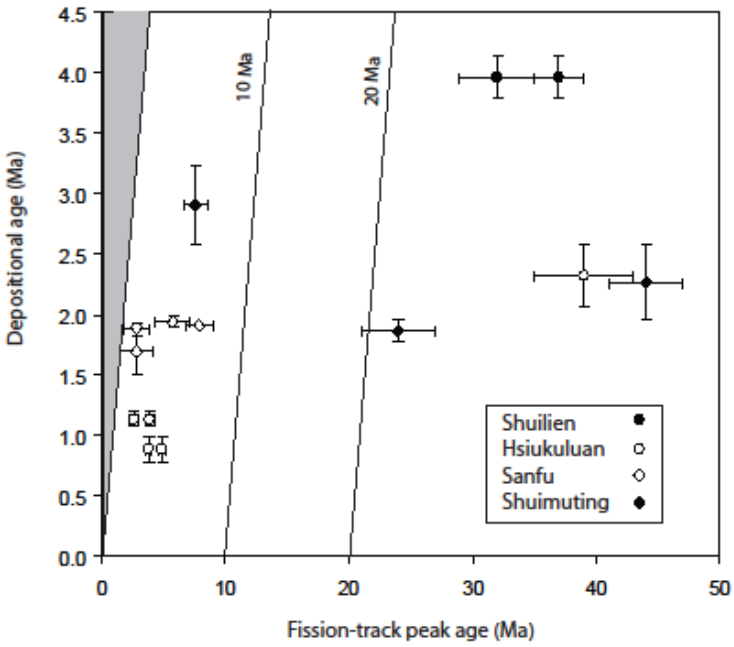

Figure 7. Plot of depositional age versus young fission-track peak age component for each of the samples measured. Lag times (near vertical lines) indicate how rapidly sample was exhumed from depth of closure of the ZFT technique to the surface and then deposited in the adjacent basin. Samples with long lag times have not been reset during the Penglai orogeny and indicate removal of cover material. Sample symbols are: Shuilien (black filled circles), Hsiukuluan (open circles), Sanfu (open diamonds) and Shuimuting (black filled diamonds).

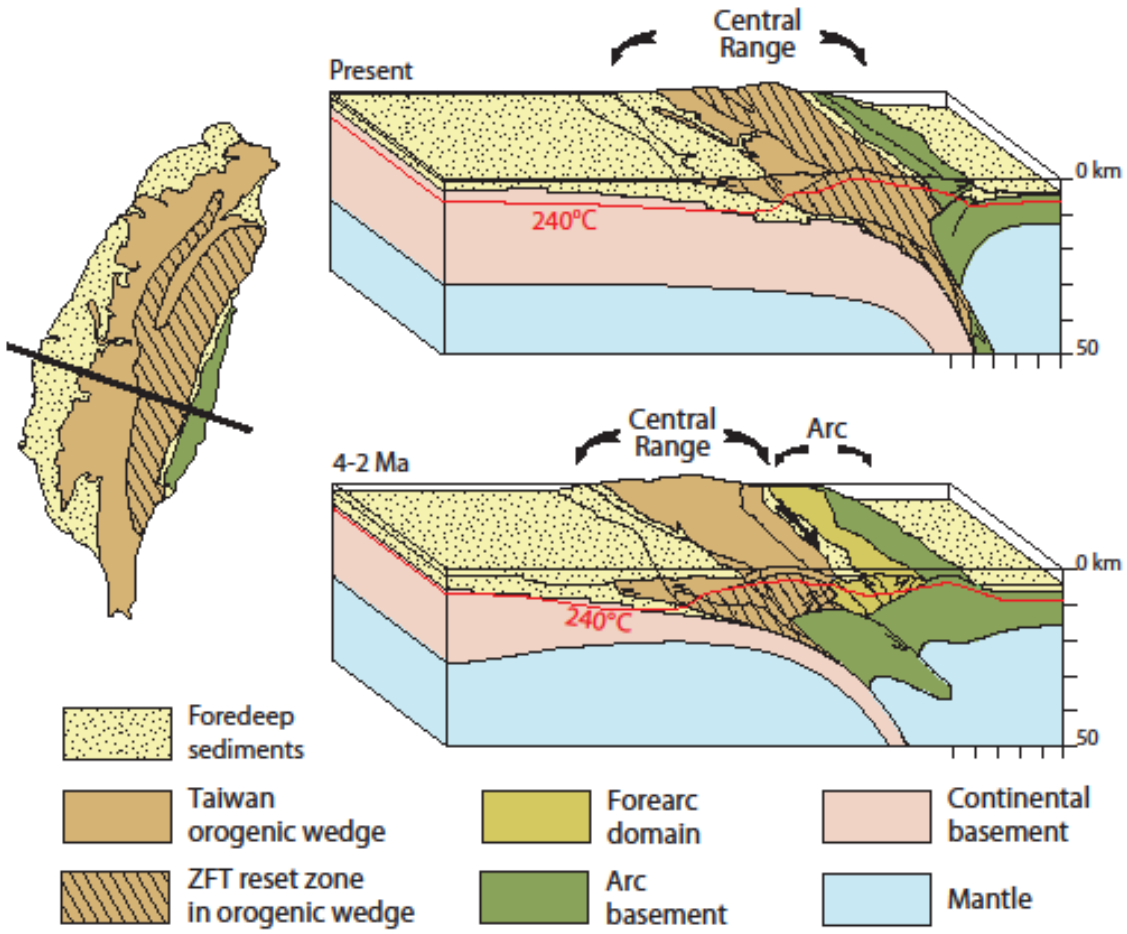

Figure 8. Schematic cross section of Taiwan pre- and post- arc-continent collision highlighting the change in the accretionary wedge through time. In the late Miocene- early Pliocene the recently emerged portion of the orogenic wedge was characterized by a subdued topography and low exhumation rates. An increase in sediment flux resulted from arc-continent collision as the sediments from the continental margin were involved in the accretionary wedge. This destabilised the wedge and resulted in increased exhumation rates from about 5-3 Ma. This increase in exhumation resulted in the exposure of reset zircon grains since late Pliocene time.

Table 1- Detrital zircon fission track data

Sample	Long. (°)	Lat. (°)	No. grains	Grain age distribution (Ma)		Age dispersion		Depositional Age (Ma)	Age components			
				Min	Max	$P\chi^2$	$RE_{\%}$		1st	2nd	3rd	4th
SH-4	23.774	121.543	50	27.2	620.2	0.0	69.8	4.13-3.79	32±3 (4%)	109±7 (22%)	265±15 (64%)	
SH-6	23.773	121.548	66	19.2	977.3	0.0	75.5	4.13-3.79	37±3 (9%)	112±6 (49%)	290±20 (42%)	
40_01	24.884	121.484	50	5.8	274.6	0.0	61.8	1.94 ± 0.5	5.7±1.4 (2%)	32±4 (18%)	72±6 (58%)	177±33 (22%)
41_01	23.450	121.487	94	2.0	801.0	0.0	87.4	1.91 ± 0.05	7.9±1.1 (17%)	50±4 (36%)	117±8 (42%)	598±137 (5%)
42_01	23.450	121.488	61	1.9	452.1	0.0	93.9	1.88 ± 0.05	2.8±0.8 (16%)	47±3 (50%)	165±12 (34%)	
43_01	23.450	121.490	60	1.2	372.8	0.0	117.4	1.70 ± 0.2	2.8±0.5 (38%)	11±1 (37%)	36±3 (20%)	335±121 (5%)
HK1	23.498	121.410	64	29	605.6	0.0	53.9	2.58-2.06	39±4 (8%)	74±5 (23%)	136±7 (55%)	310±28 (14%)
HK2	23.497	121.456	39	0.7	785.8	0.0	152.8	0.99-0.78	3.8±0.2 (80%)	134±11 (20%)		
HK3	23.503	121.439	54	2.3	178.2	0.0	129.6	0.99-0.78	4.9±0.3 (65%)	88±6 (35%)		
HK4	23.496	121.424	32	1.4	238.5	0.0	146.5	1.20-1.07	3.9±0.3 (78%)	27±1 (3%)	128±9 (19%)	
HK5	23.496	121.428	83	1.2	9.7	0.0	24.8	1.20-1.07	2.6±0.3 (51%)	4.4±4 (49%)		
SM-1	23.411	121.441	73	7.7	381.0	0.0	70.3	3.22-2.58	7.6±1 (1%)	86±5 (20%)	137±8 (43%)	275±16 (36%)
SM-6	23.405	121.453	71	22.9	1262.8	0.0	71.9	2.58-1.95	44±3 (10%)	111±4 (18%)	202±11 (54%)	506±45 (18%)
SM-9	23.409	121.468	47	24.2	903.2	0.0	65.3	1.95-1.77	24±3 (2%)	72±5 (15%)	155±13 (48%)	313±39 (35%)

SH= Shuilien samples; 4X_01= Sanfu; HK = Hsiukuluan; SM = Shuimuting. Zeta = 127±5 for SH, HK, SM samples; 341±8 for 4X_01.

Table 2- Detrital He single grain age data

Sample	Grain No.	ZFT age (Ma)	-95 Cl%	+95 Cl%	(U-Th)/He age (Ma)	± (1σ)
42_01	67	3.2	0.4	11.9	2.26	0.5
	32	3.6	0.5	7.6	3.25	0.7
	7	1.6	0.2	5.6	2.39	0.7

Table 3- Key tectonic events in the evolution of South-East China

Event	Period (Ma)	Timing
Yenshanian	150-50	Cretaceous
Indosinian	250-200	Triassic-Jurassic
Caledonian	500-400	Ordovician-Silurian
Jinningian	950-770	Proterozoic
Luliangian	2000-1800	Proterozoic

Appendix A: Supplementary data 1.
Apatite fission track grain ages.

HK1

crystal	Ng	Ns	Ni	U (ppm)		age (Ma)	error	
1		15	0	20	8.34	0.00		
2		27	18	167	38.67	25.25		6.27
3		12	20	52	27.09	89.66		23.62
4		21	4	46	13.69	20.38		10.63
5		20	0	19	5.94	0.00		
6		16	2	53	20.71	8.85		6.38
7		15	3	21	8.75	33.45		20.65
8		20	0	17	5.31	0.00		
9		30	5	291	60.64	4.03		1.82
10		12	0	3	1.56	0.00		
11		12	18	25	13.02	166.85	51.62	
12		20	27	122	38.13	51.75		11.03
13		30	1	23	4.79	10.20		10.42
14		8	14	34	26.57	95.95		30.49
15		35	0	120	21.43	0.00		
16		20	2	23	7.19	20.38		15.03
17		28	2	96	21.43	4.89		3.49
18		18	0	37	12.85	0.00		
19		18	3	240	83.35	2.93		1.70
20		20	1	57	17.82	4.12		4.15
21		40	0	50	7.81	0.00		
22		21	53	111	33.04	111.13	18.61	
23		40	5	124	19.38	9.46		4.32
24		15	1	15	6.25	15.63		4.04
25		30	0	20	4.17	0.00		
26		24	0	38	9.90	0.00		

SM1

crystal	Ng	Ns	Ni	U (ppm)		age (Ma)	error	
1		25	38	515	128.78	17.30	2.92	
2		30	5	47	9.79	24.93		11.73
3		18	7	31	10.77	52.79		22.10
4		28	0	12	2.68	0.00		
5		15	3	73	30.42	9.64		5.68
6		60	9	530	55.22	3.99		1.34
7		25	12	600	150.03	4.69	1.37	
8		10	57	65	40.63	202.65	36.87	
9		24	4	4	1.04	230.58	163.08	
10		25	7	115	28.76	14.27		5.56
11		40	3	26	4.06	27.03		16.49
12		40	6	56	8.75	25.10		10.79
13		24	17	291	75.80	13.70		3.42
14		30	0	38	7.92	0.00		
15		70	4	71	6.34	13.21		6.79
16		30	2	22	4.58	21.31		4.55

17	20	5	82	25.63	14.30	6.59
18	45	5	46	6.39	25.47	12.00
19	70	5	86	7.68	13.63	6.27
20	15	2	44	18.34	10.66	7.71

SM4

crystal	**Ng**	**Ns**	**Ni**	**U (ppm)**		**age (Ma)**	**error**
1	8	4	8	6.25		116.32	71.25
2	40	7	332	51.89		4.95	1.89
3	20	15	113	35.32		31.09	8.55
4	15	0	14	5.83		0.00	
5	15	15	219	91.27		16.06	4.29
6	15	0	17	7.08		0.00	
7	24	11	141	36.73		18.29	5.73
8	12	3	31	16.15		22.68	13.72
9	20	1	16	5		14.66	15.11
10	12	13	114	59.39		26.72	7.83
11	21	0	4	1.19		0.00	
12	18	0	10	3.47		0.00	
13	12	25	67	34.90		87.01	20.42
14	20	3	8	2.50		87.44	59.21
15	27	2	34	7.87		13.79	10.04
16	16	4	31	12.11		30.22	16.06
17	12	0	121	63.03		0.00	
18	21	12	122	36.32		23.05	2.11
19	16	6	14	5.47		99.83	48.73
20	12	6	140	72.93		10.05	4.19
21	10	2	14	8.75		33.45	25.29
22	20	15	236	73.76		14.90	3.97
23	20	3	31	9.69		22.68	13.72
24	16	11	180	70.33		14.33	1.08
25	10	15	61	38.13		57.47	16.58
26	10	2	92	57.51		5.10	3.65
27	15	0	19	7.92		0.00	
28	15	5	32	13.34		36.58	17.60

Zeta :	339±5
rho-d (CN5):	1.385E+06 tr/cm^2
Nd :	5759 tracks
U(dos):	12.0 ppm
Area 1 grat. sq.	1.386E-06

Appendix A. Supplementary Data 2

Zircon fission track data

SH4

Effective track density for fluence monitor (tracks/cm^2):	5.64E+05	
Relative error (%):		1.7
Effective uranium content of monitor (ppm):	39	
zeta factor & standard error (yr cm^2):	127	5
Size of counter square (cm^2):	1.39E-06	

Grain	RhoS	Ns	RhoI	Ni Squares		U	±2s	Grain age (Ma)	
no.	(cm^-2)	(cm^-2)		(ppm)			±95%	CI--	
1	1.60E+07	133	2.65E+06	22	6	183	77	211.7	135.6
	348								
2	1.26E+07	210	3.67E+06	61	12	254	65	121.9	91.5
	165								
3	7.15E+06	119	6.61E+06	110	12	457	88	38.6	29.4
	50.6								
4	2.22E+07	462	5.05E+06	105	15	349	69	155.1	123.9
	194.2								
5	2.72E+07	226	5.05E+06	42	6	349	108	189.3	136.4
	269.4								
6	1.90E+07	158	3.37E+06	28	6	233	88	198	133
	306.9								
7	1.33E+07	184	1.37E+06	19	10	95	43	335.3	212
	564.5								
8	1.24E+07	207	1.20E+06	20	12	83	37	357.8	229.4
	592.2								
9	7.09E+06	59	1.44E+06	12	6	100	57	171.9	92.9
	350.5								
10	1.62E+07	225	2.53E+06	35	10	175	59	225.3	158.5
	330.8								
11	1.63E+07	203	4.89E+06	61	9	338	87	117.9	88.3
	159.7								
12	1.67E+07	139	3.49E+06	29	6	241	89	168.7	113.2
	260.8								
13	1.81E+07	201	3.25E+06	36	8	225	75	196.2	138
	287.6								
14	1.37E+07	152	6.40E+06	71	8	443	106	75.9	56.7
	101.6								
15	1.05E+07	219	1.73E+06	36	15	120	40	213.5	150.6
	312								
16	1.61E+07	268	6.13E+06	102	12	424	85	93.1	73.2
	118.5								
17	2.12E+07	294	3.10E+06	43	10	215	65	239.6	174.6
	337.2								
18	1.70E+07	472	6.28E+06	174	20	434	67	96.3	79.5
	116.5								
19	9.76E+06	203	1.64E+06	34	15	113	39	209.5	146.2
	310.1								

20	7.70E+06	160	3.99E+06	83	15	276	61	68.5	51.9
	90.2								
21	2.18E+07	302	3.97E+06	55	10	274	74	193.2	145.2
	262.2								
22	1.79E+07	248	3.10E+06	43	10	215	65	202.7	147
	286.6								
23	1.46E+07	121	3.85E+06	32	6	266	94	133.5	90.3
	203.8								
24	3.01E+07	334	5.32E+06	59	8	368	96	198.3	149.2
	263.2								
25	6.76E+06	75	1.44E+06	16	8	100	49	164.4	96.1
	301.8								
26	4.37E+07	484	3.79E+06	42	8	262	81	398.6	293.4
	556.4								
27	3.46E+06	96	4.55E+06	126	20	314	57	27.3	20.7
	36								
28	2.00E+07	166	1.80E+06	15	6	125	64	380.9	229
	687								
29	1.88E+07	156	1.32E+06	11	6	91	54	482.4	270.1
	963.6								
30	1.78E+07	148	2.53E+06	21	6	175	76	246	157
	407.3								
31	1.93E+07	214	1.89E+06	21	8	131	57	352.6	228.3
	576								
32	2.06E+07	228	1.89E+06	21	8	131	57	375	243.3
	611.2								
33	2.57E+07	214	3.13E+06	26	6	216	84	286.7	192.5
	446.4								
34	1.53E+07	170	3.16E+06	35	8	218	74	171	119
	253.3								
35	4.37E+06	121	1.44E+06	40	20	100	32	107.1	74.6
	157.3								
36	7.88E+06	153	1.55E+06	30	14	107	39	179.3	121.5
	274.4								
37	8.30E+06	138	1.26E+06	21	12	87	38	229.7	146.2
	381.3								
38	1.42E+07	118	2.89E+06	24	6	200	81	172.8	111.7
	279.9								
39	1.11E+07	154	5.77E+05	8	10	40	27	643.1	332.2
	1450.5								
40	1.43E+07	198	1.66E+06	23	10	115	48	299.3	196.4
	480								
41	1.72E+07	238	1.88E+06	26	10	130	51	318	214.3
	493.6								
42	2.93E+07	244	3.49E+06	29	6	241	89	293.1	201
	444.5								
43	2.66E+07	369	1.52E+06	21	10	105	45	596.2	392.7
	955.7								
44	1.49E+07	309	1.83E+06	38	15	126	41	283.8	203.8
	407								
45	1.49E+07	309	1.54E+06	32	15	106	38	335.4	235.1
	495.7								
46	1.51E+07	188	2.00E+06	25	9	139	55	262.4	174.2
	413.8								
47	1.75E+07	194	2.53E+06	28	8	175	66	242.3	164
	372.8								

48	1.39E+07	154	1.17E+06	13	8	81	44	406.3	236.2
	768								
49	1.80E+07	150	4.57E+06	38	6	316	102	139.4	97.5
	204.6								
50	1.03E+07	129	9.62E+05	12	9	67	38	369.5	209.3
	723.1								

SH6

Effective track density for fluence monitor (tracks/cm^2): 5.63E+05

Relative error (%): 1.7

Effective uranium content of monitor (ppm): 39

zeta factor & standard error (yr cm^2): 127 5

Size of counter square (cm^2): 1.39E-06

Grain	RhoS	Ns	RhoI	Ni Squares		U	±2s	Grain age (Ma)	
no.	(cm^-2)	(cm^-2)		(ppm)			±95%	CI--	
1	1.33E+07	222	2.47E+06	41	12	171	53	190.1	136.5
	271.8								
2	1.29E+07	143	1.71E+06	19	8	119	54	261.7	163.8
	444.9								
3	1.30E+07	180	3.32E+06	46	10	230	68	138	99.7
	195.2								
4	1.67E+07	139	1.44E+06	12	6	100	57	396.5	225.4
	773.3								
5	1.48E+07	123	3.01E+06	25	6	208	83	172.6	112.6
	276.7								
6	3.51E+06	73	4.28E+06	89	15	297	63	29.3	21.1
	40.4								
7	1.80E+07	125	2.74E+06	19	5	190	86	229.4	142.7
	392								
8	1.20E+07	116	3.30E+06	32	7	228	81	127.8	86.3
	195.5								
9	1.15E+07	143	1.68E+06	21	9	117	50	237.4	151.3
	393.6								
10	2.04E+07	170	1.80E+06	15	6	125	64	389.2	234.2
	701.1								
11	1.49E+07	248	5.83E+06	97	12	404	83	90.5	70.7
	115.8								
12	3.02E+07	251	5.41E+06	45	6	375	112	195.8	142.8
	274.9								
13	1.88E+07	208	4.42E+06	49	8	306	88	149.6	109.5
	208.6								
14	4.84E+06	47	1.96E+06	19	7	136	62	87.4	50.7
	157.8								
15	1.50E+07	166	1.89E+06	21	8	131	57	274.7	176.2
	452.9								
16	7.49E+06	83	6.31E+05	7	8	44	32	402.2	193.7
	1005.1								
17	1.39E+07	116	3.85E+06	32	6	267	94	127.8	86.3
	195.5								

18	2.29E+07	317	2.60E+06	36	10	180	60	306.1	218.4
442.8									
19	2.69E+07	224	4.33E+06	36	6	300	100	217.9	153.8
318.3									
20	1.77E+07	147	1.68E+06	14	6	117	61	361.1	212.9
668.4									
21	6.49E+06	72	1.71E+06	19	8	119	54	133.2	80.2
233.9									
22	1.49E+07	206	5.70E+06	79	10	395	90	92.2	70.4
120.8									
23	1.74E+07	193	5.59E+06	62	8	387	99	110.1	82.5
149.2									
24	6.37E+06	53	7.22E+05	6	6	50	39	301.3	134.3
842.1									
25	1.33E+07	111	2.04E+06	17	6	142	68	227.5	137.7
402.6									
26	1.76E+07	219	6.01E+06	75	9	416	97	103.1	78.5
135.4									
27	1.73E+07	192	5.05E+06	56	8	350	94	121.2	89.8
166.3									
28	1.37E+07	152	5.32E+06	59	8	369	96	91.3	67.3
125.6									
29	8.30E+06	92	6.31E+06	70	8	437	105	46.8	33.9
64.9									
30	1.31E+07	109	4.93E+06	41	6	342	107	94.1	65.4
138.4									
31	2.87E+07	398	9.38E+05	13	10	65	35	999.6	602.8
1799.5									
32	1.33E+07	184	7.22E+05	10	10	50	31	617.2	340.1
1263.6									
33	1.42E+07	118	4.93E+06	41	6	342	107	101.8	71
149.1									
34	1.78E+07	197	4.33E+06	48	8	300	87	144.7	105.5
202.7									
35	1.62E+07	270	5.53E+06	92	12	383	81	103.7	80.9
132.9									
36	1.52E+07	210	3.10E+06	43	10	215	66	171.8	123.8
244.1									
37	1.98E+07	219	2.53E+06	28	8	175	66	272.4	185.2
417.4									
38	8.06E+06	67	3.25E+06	27	6	225	86	87.8	55.7
142.9									
39	1.54E+07	192	8.18E+06	102	9	566	114	66.8	51.9
86									
40	6.61E+06	55	9.62E+05	8	6	67	46	237.2	115.2
571.9									
41	1.27E+07	212	1.32E+06	22	12	92	39	333.4	217.6
539									
42	6.73E+06	140	9.14E+05	19	15	63	29	256.3	160.3
436.1									
43	1.19E+07	99	4.33E+06	36	6	300	100	97.3	66.1
146.8									
44	2.91E+07	242	2.28E+06	19	6	158	72	436.6	278.8
727.8									
45	1.95E+07	162	5.41E+06	45	6	375	112	127.1	91.2
181									

46	1.24E+07	103	3.13E+06	26	6	217	84	139.4	90.6
	223.3								
47	2.19E+07	243	3.07E+06	34	8	212	73	249.6	175.2
	367.4								
48	1.19E+07	132	2.16E+06	24	8	150	61	192.6	125.2
	310.6								
49	6.13E+06	51	2.65E+06	22	6	183	78	82	49.1
	142.1								
50	1.47E+07	122	5.05E+06	42	6	350	108	102.8	72.1
	149.7								
51	8.18E+06	68	3.25E+06	27	6	225	86	89.1	56.5
	144.9								
52	1.41E+07	117	1.19E+07	99	6	825	168	42.1	31.8
	55.6								
53	4.91E+06	68	6.49E+05	9	10	45	29	260.6	132.7
	588.7								
54	2.31E+06	77	4.51E+06	150	24	312	52	18.4	13.8
	24.5								
55	1.01E+07	140	6.20E+06	86	10	430	94	57.8	43.7
	76.4								
56	2.04E+07	339	4.99E+06	83	12	346	77	143.7	111.8
	184.7								
57	1.72E+07	143	2.04E+06	17	6	142	68	291.5	178.6
	510.4								
58	8.12E+06	90	3.70E+06	41	8	256	80	77.8	53.4
	115.6								
59	1.08E+07	149	3.32E+06	46	10	230	68	114.5	82
	163.1								
60	1.75E+07	194	5.41E+06	60	8	375	97	114.4	85.4
	155.5								
61	2.10E+07	175	6.25E+06	52	6	433	120	118.9	87.1
	165.5								
62	1.55E+07	129	2.65E+06	22	6	183	78	205	131.2
	337.6								
63	1.46E+07	121	2.53E+06	21	6	175	76	201.5	127.4
	336.3								
64	1.97E+07	246	1.76E+06	22	9	122	52	385.3	252.7
	619.7								
65	6.94E+06	77	5.14E+06	57	8	356	95	48.1	33.7
	69								
66	9.83E+06	109	3.07E+06	34	8	212	73	113.2	76.8
	171.7								

40-01

Effective track density for fluence monitor (tracks/cm^2):	2.79E+05	
Relative error (%):		1.98
Effective uranium content of monitor (ppm):	12.3	
zeta factor & standard error (yr cm^2):	341.75	7.81
Size of counter square (cm^2):	6.58E-07	

Grain	RhoS	Ns	RhoI	Ni Squares		U	±2s	Grain age (Ma)	
no.	(cm^-2)	(cm^-2)		(ppm)			±95%	CI--	
1	2.74E+06	18	9.12E+05	6	10	40	32	138.9	54.1
	425.9								
2	4.56E+06	12	6.84E+06	18	4	302	141	31.8	13.9
	69.4								
3	3.04E+06	24	3.04E+06	24	12	134	54	47.5	25.8
	87.2								
4	5.83E+06	46	1.01E+06	8	12	45	31	264	126.6
	640								
5	8.74E+06	23	6.84E+06	18	4	302	141	60.5	31.3
	118.8								
6	2.03E+06	16	5.07E+05	4	12	22	21	182.5	61.1
	739.8								
7	3.04E+06	12	1.27E+06	5	6	56	48	111.3	37.4
	401.9								
8	8.36E+06	33	4.31E+06	17	6	190	91	91.4	49.8
	174.9								
9	7.60E+05	3	2.03E+06	8	6	89	61	18.4	3.1
	74.1								
10	6.84E+06	45	4.71E+06	31	10	208	75	68.7	42.6
	112.3								
11	4.56E+06	18	3.04E+06	12	6	134	76	70.8	32.5
	160.8								
12	8.11E+06	32	4.56E+06	18	6	201	94	83.8	45.9
	158.5								
13	8.11E+06	32	3.55E+06	14	6	156	82	107.3	56.2
	217.5								
14	1.27E+06	20	1.07E+07	169	24	472	75	5.7	3.4
	9								
15	7.22E+06	57	4.43E+06	35	12	196	66	77	49.8
	120.9								
16	1.44E+07	57	5.07E+06	20	6	223	99	133.7	79.7
	234.7								
17	3.59E+06	85	5.36E+06	127	36	237	43	31.9	24.1
	42.1								
18	1.65E+06	26	7.60E+05	12	24	34	19	101.7	50
	221								
19	1.60E+07	42	9.12E+06	24	4	402	163	82.6	49.1
	142.6								
20	5.32E+06	42	7.35E+06	58	12	324	86	34.5	22.5
	52.1								
21	2.70E+06	16	4.56E+06	27	9	201	77	28.3	14.2
	54.2								
22	6.27E+06	99	5.45E+06	86	24	240	53	54.6	40.4
	73.9								
23	1.52E+07	40	9.12E+06	24	4	402	163	78.7	46.5
	136.5								
24	6.08E+06	24	3.04E+06	12	6	134	76	94	45.6
	206.1								
25	9.88E+06	26	1.52E+06	4	4	67	63	292.8	106.5
	1119								
26	3.04E+06	8	1.52E+06	4	4	67	63	92.8	25.5
	418.8								

27	7.09E+06	28	3.55E+06	14	6	156	82	94.1	48.3
	193.2								
28	6.59E+06	39	3.55E+06	21	9	156	68	87.6	50.5
	156.7								
29	1.06E+07	42	4.81E+06	19	6	212	97	104	59.6
	189.2								
30	1.52E+06	18	3.97E+06	47	18	175	51	18.3	10
	32								
31	9.39E+06	68	9.12E+06	66	11	402	100	48.9	34.3
	69.7								
32	6.08E+06	24	5.07E+06	20	6	223	99	56.9	30.2
	108.4								
33	5.57E+06	33	2.87E+06	17	9	127	61	91.4	49.8
	174.9								
34	6.84E+06	54	1.27E+06	10	12	56	35	249	128.3
	543.8								
35	3.55E+06	14	1.77E+06	7	6	78	57	93.5	35.9
	273.4								
36	1.82E+07	48	5.70E+06	15	4	251	128	149.6	83.3
	287.1								
37	1.10E+07	29	8.74E+06	23	4	384	159	60	33.6
	108.4								
38	1.05E+07	62	1.86E+06	11	9	82	48	261.1	139.1
	545								
39	2.79E+06	11	7.60E+05	3	6	33	36	166.9	46.1
	912.2								
40	3.21E+06	19	2.53E+06	15	9	111	57	60.2	29.1
	127.1								
41	9.37E+06	37	6.33E+06	25	6	278	111	70.3	41.3
	121.8								
42	1.44E+07	57	6.08E+06	24	6	267	108	112.2	68.9
	189								
43	1.62E+07	64	4.05E+06	16	6	178	88	187.2	108.2
	345.8								
44	7.09E+06	28	9.88E+06	39	6	434	139	34.3	20.3
	57.1								
45	4.73E+06	28	3.38E+06	20	9	148	66	66.5	36.3
	124.4								
46	2.66E+06	28	3.13E+06	33	16	138	48	40.5	23.6
	69								
47	5.70E+06	15	4.94E+06	13	4	217	118	54.9	24.4
	125								
48	7.22E+06	19	6.46E+06	17	4	284	136	53.2	26.2
	108.7								
49	4.81E+06	19	1.77E+06	7	6	78	57	126.8	52
	355.9								
50	3.55E+06	14	6.08E+06	24	6	267	108	28	13.3
	56								

41-01

Effective track density for fluence monitor (tracks/cm^2): 2.75E+05

Relative error (%): 1.9

Effective uranium content of monitor (ppm): 12.3

zeta factor & standard error (yr cm^2): 341.75 7.81

Size of counter square (cm^2): 6.58E-07

Grain	RhoS	Ns	RhoI	Ni Squares		U	±2s	Grain age (Ma)	
no.	(cm^-2)	(cm^-2)		(ppm)			±95%	CI--	
1	6.59E+06	26	5.07E+06	20	6	226	100	60.7	32.7
	114.6								
2	6.27E+06	33	3.23E+06	17	8	144	69	90.2	49.1
	172.6								
3	5.07E+06	20	4.81E+06	19	6	215	98	49.3	25
	97.4								
4	7.60E+05	4	2.28E+06	12	8	102	58	16.1	3.7
	51.5								
5	2.39E+07	63	1.14E+06	3	4	51	55	877.3	314.6
	3654.8								
6	1.48E+07	39	6.84E+06	18	4	306	143	100.6	56.6
	186.7								
7	3.80E+06	15	3.55E+06	14	6	159	83	50.1	22.6
	111.8								
8	5.51E+06	58	2.37E+06	25	16	106	42	107.8	66.7
	179.7								
9	1.03E+07	27	4.18E+06	11	4	187	110	113.4	55.1
	253								
10	3.29E+06	26	1.39E+06	11	12	62	37	109.2	52.8
	244.7								
11	9.12E+06	96	4.75E+06	50	16	212	60	89.5	63
	128.7								
12	4.05E+05	4	5.07E+05	5	15	23	19	37.8	7.5
	172.5								
13	3.04E+06	16	4.75E+06	25	8	212	84	30.1	15
	58.4								
14	6.27E+06	33	6.08E+06	32	8	272	96	48.3	28.8
	81.1								
15	9.50E+06	100	7.98E+06	84	16	357	79	55.7	41.2
	75.5								
16	1.04E+07	41	1.01E+06	4	6	45	43	449	172
	1629								
17	2.15E+06	17	1.14E+06	9	12	51	33	87.5	37.3
	222.4								
18	7.60E+05	8	4.84E+06	51	16	217	61	7.5	3
	15.7								
19	3.70E+06	39	4.94E+06	52	16	221	62	35.2	22.6
	54.3								
20	2.53E+06	10	4.31E+06	17	6	193	92	27.8	11.3
	63.7								
21	3.04E+06	18	2.20E+06	13	9	98	54	64.5	30.1
	143.1								
22	3.29E+06	13	1.27E+06	5	6	57	48	118.8	40.7
	423.9								
23	2.89E+05	4	6.51E+05	9	21	29	19	21.3	4.7
	74.5								

24	2.77E+07	73	6.08E+06	16	4	272	134	209.3	122.3
	383.7								
25	1.33E+06	7	6.08E+06	32	8	272	96	10.5	3.8
	23.7								
26	2.53E+06	10	1.01E+06	4	6	45	43	113.8	33.8
	494.3								
27	1.52E+07	40	5.70E+06	15	4	255	130	123.3	67.3
	240.1								
28	1.24E+07	49	2.79E+06	11	6	125	74	203.8	106.4
	432.3								
29	7.22E+06	57	2.79E+06	22	12	125	53	120.1	72.8
	206.2								
30	6.84E+06	54	4.05E+06	32	12	181	64	78.7	50
	125.9								
31	1.13E+07	67	3.38E+06	20	9	151	67	154.7	93.6
	268.7								
32	7.90E+06	52	3.95E+06	26	10	177	69	93.1	57.3
	155.2								
33	7.60E+06	30	2.53E+06	10	6	113	70	138	66.7
	315.9								
34	2.85E+06	15	2.09E+06	11	8	93	55	63.5	27.4
	152.6								
35	5.51E+06	29	1.14E+06	6	8	51	40	218.7	91.9
	637.3								
36	1.49E+07	59	4.31E+06	17	6	193	92	160	93
	292.2								
37	5.07E+05	5	1.11E+06	11	15	50	29	21.7	5.8
	66.4								
38	1.39E+07	55	6.59E+06	26	6	294	115	98.4	60.9
	163.4								
39	6.75E+05	4	8.95E+06	53	9	400	110	3.7	0.9
	9.6								
40	1.47E+07	58	6.08E+06	24	6	272	110	112.2	69
	188.7								
41	2.03E+05	2	2.84E+06	28	15	127	48	3.6	0.4
	13.3								
42	1.29E+07	34	6.84E+06	18	4	306	143	87.8	48.5
	165.1								
43	8.36E+06	33	3.55E+06	14	6	159	83	109.1	57.4
	220.6								
44	1.90E+06	20	3.32E+06	35	16	149	50	26.9	14.7
	47.7								
45	3.23E+06	17	1.90E+06	10	8	85	53	78.9	34.4
	192.6								
46	1.33E+06	7	1.14E+06	6	8	51	40	54.4	15.8
	194.7								
47	6.25E+06	37	7.43E+06	44	9	332	100	39.4	24.7
	62.4								
48	3.67E+06	29	3.29E+06	26	12	147	57	52.2	29.7
	92.2								
49	2.03E+06	8	9.37E+06	37	6	419	138	10.3	4.1
	22.2								
50	3.80E+06	10	4.94E+06	13	4	221	121	36.2	14.2
	88.8								
51	7.35E+06	29	8.36E+06	33	6	374	130	41.2	24.1
	69.9								

52	9.50E+06	75	5.07E+05	4	12	23	21	797.7	321.8
	2678.7								
53	8.44E+05	5	1.52E+06	9	9	68	44	26.4	6.9
	86.3								
54	1.90E+06	5	6.46E+06	17	4	289	139	14.1	4
	39								
55	5.83E+06	23	1.52E+06	6	6	68	53	174.3	70.9
	519.9								
56	1.71E+07	45	1.90E+06	5	4	85	73	398.7	166.2
	1239.5								
57	1.04E+07	41	6.33E+06	25	6	283	113	76.4	45.5
	131.2								
58	5.70E+05	3	7.79E+06	41	8	348	109	3.6	0.7
	10.8								
59	9.50E+05	5	3.80E+05	2	8	17	21	111.6	19.2
	1129.7								
60	1.69E+05	1	5.07E+05	3	9	23	24	17.1	0.3
	192.4								
61	2.17E+05	2	2.06E+06	19	14	92	42	5.3	0.6
	20.5								
62	2.53E+06	10	3.80E+06	15	6	170	87	31.4	12.6
	74.2								
63	7.22E+06	19	6.46E+06	17	4	289	139	52.3	25.8
	106.8								
64	1.14E+06	6	5.70E+06	30	8	255	93	9.6	3.2
	22.9								
65	8.61E+06	34	7.09E+06	28	6	316	119	57	33.6
	97.6								
66	1.52E+07	60	3.80E+06	15	6	169	86	184.7	104.9
	349								
67	3.80E+06	40	1.04E+06	11	16	47	27	167.7	85.8
	361.2								
68	1.14E+07	45	7.60E+06	30	6	338	123	70.3	43.4
	115.6								
69	2.28E+06	9	1.01E+06	4	6	45	43	103.2	29.6
	455.9								
70	1.17E+07	46	7.09E+06	28	6	316	119	76.9	47.2
	127.8								
71	1.49E+07	59	7.09E+06	28	6	316	119	98.4	62
	160.3								
72	2.85E+06	30	2.09E+06	22	16	93	39	64	35.8
	116.3								
73	1.33E+07	79	5.40E+06	32	9	241	85	115.2	75.8
	179.5								
74	1.14E+06	6	7.60E+05	4	8	34	32	69.6	16.8
	332.8								
75	2.53E+05	1	1.77E+06	7	6	79	58	7.6	0.1
	52.3								
76	2.89E+07	76	2.28E+06	6	4	101	80	558.7	256.9
	1494.8								
77	1.01E+06	4	1.77E+06	7	6	79	58	27.4	5.8
	105.4								
78	1.11E+06	11	2.94E+06	29	15	131	48	18.1	8.1
	36.9								
79	3.04E+06	40	2.05E+06	27	20	91	35	69.5	41.7
	117.7								

80	7.35E+06	58	1.90E+06	15	12	85	43	178.6	101.2
	338.3								
81	3.55E+06	28	7.60E+05	6	12	34	27	212.3	88.8
	620.6								
82	3.80E+06	15	4.31E+06	17	6	192	92	41.6	19.3
	88.2								
83	1.50E+07	79	4.37E+06	23	8	195	81	159.4	99.9
	265.4								
84	1.20E+07	79	3.50E+06	23	10	156	64	159.4	99.9
	265.4								
85	3.19E+06	21	2.58E+06	17	10	115	55	58	29.2
	116.8								
86	1.60E+07	63	1.06E+07	42	6	474	146	70.4	46.9
	106.6								
87	1.39E+06	11	4.81E+06	38	12	214	70	13.8	6.3
	27.3								
88	7.09E+06	28	5.83E+06	23	6	259	107	57.2	31.8
	103.8								
89	3.21E+06	19	2.03E+06	12	9	90	51	74	34.3
	166.9								
90	2.53E+05	2	7.47E+06	59	12	333	87	1.7	0.2
	6								
91	1.09E+07	43	4.81E+06	19	6	214	97	105.5	60.6
	191.6								
92	1.01E+06	8	5.45E+06	43	12	242	74	8.9	3.6
	18.9								
93	5.89E+06	31	6.08E+06	32	8	271	96	45.6	26.9
	77.1								
94	4.18E+06	33	2.03E+06	16	12	90	45	96.2	51.8
	187								

42-01

Effective track density for fluence monitor (tracks/cm^2): 2.75E+05

Relative error (%:) 1.85

Effective uranium content of monitor (ppm): 12.3

zeta factor & standard error (yr cm^2): 341.75 7.81

Size of counter square (cm^2): 6.58E-07

Grain	RhoS	Ns	RhoI	Ni Squares	U	±2s	Grain age (Ma)	
no.	(cm^-2)	(cm^-2)		(ppm)		±95%	CI--	
1	6.27E+06	99	1.96E+06	31	24	88	32	147.6	98.3
	228.5								
2	5.57E+06	44	5.07E+06	40	12	227	72	51.4	32.7
	80.9								
3	8.74E+06	69	5.83E+06	46	12	261	77	69.9	47.5
	103.9								
4	2.79E+06	22	3.17E+06	25	12	142	56	41.2	22.1
	76								
5	4.56E+06	36	5.32E+06	42	12	238	74	40.1	25
	64.1								

6	5.91E+06	35	1.86E+06	11	9	83	49	146.1	73.6
318.3									
7	7.22E+06	57	8.49E+06	67	12	380	94	39.8	27.4
57.6									
8	8.23E+06	65	7.35E+06	58	12	329	87	52.4	36.2
76									
9	8.87E+05	7	2.41E+06	19	12	108	49	17.5	6.1
42.9									
10	5.07E+05	4	2.15E+06	17	12	96	46	11.4	2.7
33.8									
11	5.74E+06	34	3.38E+06	20	9	151	67	79	44.4
144.8									
12	1.44E+07	85	2.87E+06	17	9	129	62	228.7	136.6
408.7									
13	3.80E+05	3	1.11E+07	88	12	499	108	1.7	0.3
4.8									
14	2.18E+06	23	4.65E+06	49	16	208	60	22.1	12.8
36.8									
15	2.20E+06	13	3.55E+06	21	9	159	69	29.1	13.3
60.6									
16	1.27E+05	2	1.58E+06	25	24	71	28	4	0.4
15.1									
17	2.41E+06	19	2.28E+06	18	12	102	48	49.3	24.5
99.4									
18	2.17E+05	2	8.68E+05	8	14	39	27	12.4	1.2
58.6									
19	0.00E+00	0	1.52E+06	4	4	68	64	8.9	0.3
70.7									
20	3.80E+05	3	7.22E+06	57	12	323	86	2.6	0.5
7.6									
21	1.25E+07	33	8.74E+06	23	4	391	162	66.8	38.2
119.2									
22	1.90E+07	75	5.07E+06	20	6	227	101	172.6	105.3
297.8									
23	2.05E+07	54	4.56E+06	12	4	204	116	205.6	110.5
420.2									
24	4.81E+06	38	6.08E+06	48	12	272	79	37.1	23.5
57.9									
25	1.75E+07	46	5.70E+06	15	4	255	130	141.3	78.3
272									
26	5.74E+06	34	4.73E+06	28	9	212	80	56.7	33.4
97									
27	1.48E+07	39	2.66E+06	7	4	119	87	251.6	114.5
658.5									
28	2.28E+06	9	5.07E+05	2	6	23	29	196.4	43.5
1749									
29	2.56E+06	27	1.14E+06	12	16	51	29	104	51.5
225.1									
30	8.74E+06	23	5.32E+06	14	4	238	125	76.3	37.9
160.2									
31	1.27E+05	1	2.41E+06	19	12	108	49	2.8	0.1
15.5									
32	6.84E+06	27	7.85E+06	31	6	352	126	40.8	23.4
70.5									
33	5.74E+06	34	5.40E+06	32	9	242	85	49.7	29.7
83.1									

34	5.07E+06	20	4.56E+06	18	6	204	95	51.9	26.1
103.8									
35	2.28E+07	60	7.60E+06	20	4	340	151	138.5	83
242.3									
36	7.35E+06	29	3.04E+06	12	6	136	77	111.5	55.8
239.8									
37	2.75E+06	29	1.80E+06	19	16	81	37	71	38.7
133.9									
38	1.90E+07	75	5.83E+06	23	6	261	108	150.5	94
251.3									
39	3.38E+06	20	3.21E+06	19	9	144	65	49.2	25
97.2									
40	0.00E+00	0	1.27E+06	10	12	57	35	3.4	0.1
20.9									
41	3.29E+06	13	3.80E+06	15	6	170	87	40.6	17.8
91.1									
42	2.03E+05	2	3.14E+06	31	15	141	50	3.2	0.4
11.9									
43	1.16E+07	61	1.04E+07	55	8	468	127	51.8	35.4
76									
44	2.03E+06	12	2.03E+06	12	9	91	51	46.8	19.2
113.3									
45	5.57E+06	22	5.32E+06	21	6	238	103	49	25.7
93.4									
47	7.05E+06	51	3.04E+06	22	11	138	58	106.1	63.6
183.7									
48	2.91E+06	23	1.27E+06	10	12	57	36	104.8	48.6
246.5									
49	2.36E+07	62	6.08E+06	16	4	276	136	175.9	101.5
325.6									
50	7.60E+06	20	2.28E+06	6	4	103	81	149.9	59.5
454.2									
51	1.94E+07	51	6.84E+06	18	4	310	145	129.3	74.9
234.9									
52	2.87E+06	17	2.36E+06	14	9	107	56	55.9	26
122.3									
53	8.44E+04	2	2.62E+06	62	36	119	30	1.6	0.2
5.6									
54	2.75E+06	29	2.28E+06	24	16	103	42	55.7	31.4
99.9									
55	4.05E+06	16	4.31E+06	17	6	195	94	43.5	20.6
91.3									
56	1.90E+07	50	4.56E+06	12	4	207	117	188.4	100.5
387.1									
57	1.04E+07	55	9.50E+05	5	8	43	37	477.3	202.4
1456.1									
58	5.07E+05	2	1.52E+06	6	6	69	54	16.2	1.5
85.9									
59	1.55E+07	61	3.55E+06	14	6	161	85	197.2	110.6
380.1									
60	4.56E+05	3	2.13E+06	14	10	96	51	10.3	1.8
35.5									
61	6.08E+06	72	7.26E+06	86	18	329	72	38.7	27.9
53.6									

43-01

Effective track density for fluence monitor (tracks/cm^2): 2.60E+05

Relative error (%): 1.71

Effective uranium content of monitor (ppm): 12.3

zeta factor & standard error (yr cm^2): 341.75 7.81

Size of counter square (cm^2): 6.58E-07

Grain	RhoS	Ns	RhoI	Ni Squares		U	±2s	Grain age (Ma)	
no.	(cm^-2)	(cm^-2)		(ppm)			±95%	CI--	
1	1.27E+06	10	6.46E+06	51	12	305	86	8.8	3.9
	17.4								
2	1.90E+05	1	1.04E+07	55	8	494	134	0.9	0
	4.7								
3	4.18E+06	11	1.25E+07	33	4	593	206	14.9	6.7
	30								
4	1.14E+06	3	8.36E+06	22	4	395	167	6.3	1.2
	20.2								
5	3.80E+06	10	1.41E+07	37	4	665	218	12.1	5.3
	24.6								
6	7.60E+05	4	3.99E+06	21	8	189	82	8.7	2.1
	25.1								
7	1.03E+07	27	9.88E+06	26	4	467	182	46	25.8
	81.9								
8	5.07E+05	2	3.55E+06	14	6	168	88	6.8	0.7
	27.6								
9	0.00E+00	0	1.77E+06	7	6	84	61	4.6	0.2
	30.8								
10	9.12E+05	6	4.86E+06	32	10	230	81	8.5	2.8
	20.2								
11	2.62E+06	31	3.46E+06	41	18	164	51	33.6	20.3
	54.8								
12	7.60E+05	8	4.56E+06	48	16	216	62	7.5	3
	15.8								
13	2.15E+06	17	6.08E+06	48	12	287	83	15.8	8.5
	27.8								
14	5.07E+05	4	5.07E+05	4	12	24	23	44.3	8.3
	234.4								
15	1.65E+06	13	2.91E+06	23	12	138	57	25.2	11.7
	51.6								
16	3.80E+05	1	6.08E+06	16	4	287	142	3.2	0.1
	17.9								
17	0.00E+00	0	1.77E+06	7	6	84	61	4.6	0.2
	30.8								
18	0.00E+00	0	3.04E+06	12	6	144	81	2.6	0.1
	16								
19	1.01E+07	40	1.52E+06	6	6	72	56	283.4	123.5
	803.5								
20	2.53E+05	1	1.27E+06	5	6	60	51	9.9	0.2
	79								
21	7.60E+05	3	4.31E+06	17	6	204	98	8.2	1.5
	27.1								

22	7.60E+05	3	5.32E+06	21	6	252	109	6.6	1.2
21.2									
23	1.90E+06	15	3.29E+06	26	12	156	61	25.7	12.6
50.1									
24	2.53E+06	15	4.56E+06	27	9	216	83	24.8	12.2
48									
25	1.77E+06	7	7.35E+06	29	6	347	128	10.9	4
25									
26	1.56E+07	41	7.98E+06	21	4	377	163	85.9	49.9
152.9									
27	1.69E+05	1	3.55E+06	21	9	168	73	2.4	0.1
13.2									
28	3.38E+05	2	5.91E+06	35	9	279	94	2.7	0.3
9.9									
29	2.43E+05	4	8.51E+05	14	25	40	21	13	3
40.3									
30	1.27E+06	5	5.57E+06	22	6	264	111	10.3	3
27.3									
31	1.69E+05	1	8.61E+06	51	9	407	114	1	0
5.1									
32	7.24E+04	1	8.68E+05	12	21	41	23	4.2	0.1
25									
33	7.60E+05	3	9.12E+06	36	6	431	144	3.9	0.7
11.7									
34	2.03E+06	8	5.57E+06	22	6	264	111	16.4	6.2
37.6									
35	0.00E+00	0	4.94E+06	13	4	234	127	2.4	0.1
14.6									
36	7.24E+04	1	2.75E+06	38	21	130	42	1.3	0
6.9									
37	6.08E+06	16	4.94E+06	13	4	234	127	54.4	24.6
122.6									
38	2.53E+05	1	3.04E+06	12	6	144	81	4.2	0.1
25									
39	8.74E+06	23	8.36E+06	22	4	395	167	46.3	24.7
86.9									
40	1.33E+06	7	5.13E+06	27	8	243	93	11.7	4.2
27.1									
41	3.29E+06	13	5.32E+06	21	6	252	109	27.6	12.6
57.4									
42	5.07E+05	3	9.46E+06	56	9	447	120	2.5	0.5
7.3									
43	2.53E+05	1	6.08E+06	24	6	287	117	2.1	0
11.4									
44	1.01E+06	4	1.37E+07	54	6	647	177	3.4	0.9
8.9									
45	5.07E+05	3	5.74E+06	34	9	272	93	4.1	0.8
12.5									
46	5.07E+06	20	3.80E+06	15	6	179	91	59.1	28.9
124									
47	1.90E+05	1	1.90E+06	10	8	89	55	5	0.1
31.3									
48	5.70E+05	3	7.60E+05	4	8	36	34	33.8	4.9
195.2									
49	5.57E+05	11	2.53E+06	50	30	119	34	9.9	4.6
19.1									

50	1.69E+05	1	3.71E+06	22	9	175	74	2.3	0
	12.6								
51	2.24E+06	53	3.80E+06	90	36	179	38	26.3	18.3
	37.3								
52	1.52E+05	3	2.43E+06	48	30	114	33	2.9	0.6
	8.7								
53	3.04E+05	3	3.44E+06	34	15	162	55	4.1	0.8
	12.5								
54	2.03E+06	12	7.77E+06	46	9	366	108	11.8	5.6
	22.3								
55	3.04E+06	12	8.11E+06	32	6	381	134	16.9	7.8
	33.4								
56	3.55E+06	21	3.38E+05	2	9	16	20	424.2	113.6
3190.3									
57	2.28E+06	9	2.53E+05	1	6	12	19	347.4	55.4
	8493.4								
58	2.53E+05	3	4.90E+06	58	18	230	61	2.4	0.5
	7.1								
59	1.27E+06	5	1.14E+07	45	6	536	160	5.1	1.5
	12.5								
60	1.77E+06	7	9.88E+06	39	6	465	149	8.2	3
	18.1								

HK1

Effective track density for fluence monitor (tracks/cm^2):	5.23E+05	
Relative error (%):		1.7
Effective uranium content of monitor (ppm):	39	
zeta factor & standard error (yr cm^2):	127	5
Size of counter square (cm^2):	1.39E-06	

Grain	RhoS	Ns	RhoI	Ni Squares		U	±2s	Grain age (Ma)	
no.	(cm^-2)	(cm^-2)		(ppm)			±95%	CI--	
1	8.44E+06	117	4.62E+06	64	10	344	87	60.4	44.2
	83.3								
2	7.79E+06	108	1.88E+06	26	10	140	55	135.9	88.5
	217.2								
3	1.47E+07	122	2.77E+06	23	6	206	85	172.8	111
	282.4								
4	4.47E+06	62	1.37E+06	19	10	102	46	106.8	63.6
	189.3								
5	2.00E+07	222	2.16E+06	24	8	161	65	298.3	197.8
	472.6								
6	3.29E+07	456	1.05E+07	146	10	786	133	102.7	83.8
	125.7								
7	1.83E+07	152	5.65E+06	47	6	421	123	106.3	76.4
	150.8								
8	1.45E+07	201	3.68E+06	51	10	274	77	129.3	94.9
	179.5								
9	7.22E+06	90	5.93E+06	74	9	442	104	40.3	29.2
	55.6								

10	7.94E+06	110	3.54E+06	49	10	264	75	74	52.5
106									
11	1.33E+07	148	4.33E+06	48	8	323	93	101.4	72.9
143.6									
12	1.50E+07	125	3.37E+06	28	6	251	94	145.9	96.9
228.3									
13	8.66E+06	96	9.92E+05	11	8	74	44	279.9	152.9
574.2									
14	1.08E+07	150	4.47E+06	62	10	334	85	79.7	59
109.1									
15	2.38E+07	297	5.45E+06	68	9	407	99	142.6	108.6
187.3									
16	9.30E+06	116	2.65E+06	33	9	197	68	115.3	78.1
175.3									
17	1.78E+07	296	4.69E+06	78	12	350	80	124.2	95.8
161.1									
18	1.06E+07	118	3.16E+06	35	8	235	79	110.6	75.6
166.4									
19	1.49E+07	207	6.85E+06	95	10	511	106	71.8	55.6
92.6									
20	2.33E+07	388	3.07E+06	51	12	229	64	247.2	185.2
337									
21	1.06E+07	176	2.47E+06	41	12	184	57	140.6	100
202.6									
22	9.43E+06	183	3.66E+06	71	14	273	65	84.7	63.7
112.5									
23	1.97E+07	164	1.13E+07	94	6	843	176	57.6	44.1
75									
24	1.97E+07	218	5.95E+06	66	8	444	110	108.2	81.4
143.8									
25	8.75E+06	97	6.67E+06	74	8	498	117	43.4	31.7
59.6									
26	1.11E+07	185	2.89E+06	48	12	215	62	126.4	91.9
177.6									
27	1.89E+07	210	4.51E+06	50	8	336	95	137.7	101
191.4									
28	3.09E+07	428	8.66E+06	120	10	646	120	117	94.2
145.3									
29	1.80E+07	250	4.18E+06	58	10	312	82	141.3	106.1
191.4									
30	1.16E+07	129	1.62E+06	18	8	121	56	231.9	143
402									
31	2.31E+07	256	8.48E+06	94	8	632	132	89.5	69.8
114.8									
32	3.49E+07	290	7.46E+06	62	6	556	142	152.5	114.9
202.2									
33	1.75E+07	194	7.85E+06	87	8	585	127	73.4	56.3
95.6									
34	3.01E+07	334	5.77E+06	64	8	430	108	170	128.9
223.8									
35	3.93E+07	327	4.81E+06	40	6	359	113	265	191.9
376.5									
36	2.81E+07	234	4.57E+06	38	6	341	110	200.6	142.8
290.1									
37	2.53E+07	210	4.81E+06	40	6	359	113	171.5	122.5
246.7									

38	1.44E+07	160	3.43E+06	38	8	256	83	137.9	96.8
201.9									
39	1.59E+07	132	9.14E+06	76	6	681	158	57.3	42.7
76.7									
40	1.44E+07	120	2.77E+06	23	6	206	85	170	109.2
278									
41	2.57E+07	214	4.81E+06	40	6	359	113	174.7	124.8
251.2									
42	5.70E+06	79	3.61E+06	50	10	269	76	52.2	36.2
76									
43	2.15E+07	179	4.09E+06	34	6	305	104	171.8	119.3
255.6									
44	5.91E+06	131	3.61E+06	80	16	269	61	54	40.5
72.1									
45	1.73E+07	192	1.71E+06	19	8	128	58	324.7	205.5
546.5									
46	8.54E+06	71	1.68E+06	14	6	126	66	164.7	93.3
316									
47	6.65E+06	129	2.63E+06	51	14	196	55	83.3	59.9
117.7									
48	7.67E+06	85	2.89E+06	32	8	215	76	87.3	57.8
135.7									
49	6.35E+06	88	7.36E+06	102	10	549	110	28.6	21.2
38.5									
50	1.95E+07	162	9.62E+05	8	6	72	49	628.1	324.6
1417.5									
51	1.39E+07	192	2.81E+06	39	10	210	67	160.9	114.2
233.1									
52	1.08E+07	150	2.67E+06	37	10	199	65	132.8	92.6
195.8									
53	1.32E+07	220	5.23E+06	87	12	390	84	83.2	64.1
107.8									
54	9.92E+06	165	8.42E+06	140	12	628	108	39	30.7
49.5									
55	1.64E+07	273	3.73E+06	62	12	278	71	143.7	108.1
190.9									
56	1.47E+07	204	1.30E+06	18	10	97	45	362.9	227.8
618									
57	2.09E+07	290	6.06E+06	84	10	452	100	113.2	87.7
145.9									
58	3.08E+07	384	5.93E+06	74	9	442	104	169.2	130.6
219									
59	2.24E+07	186	6.01E+06	50	6	448	127	122.1	89.2
170.4									
60	1.44E+07	199	2.89E+06	40	10	215	68	162.6	115.9
234.3									
61	1.48E+07	123	4.81E+06	40	6	359	113	101	70.4
148.3									
62	9.56E+06	106	3.07E+06	34	8	229	78	102.4	69.3
155.5									
63	3.28E+07	273	2.16E+06	18	6	161	75	481	304.9
810.5									
64	2.42E+07	201	1.01E+07	84	6	753	166	78.7	60.3
102.7									

HK2

Effective track density for fluence monitor (tracks/cm^2): 5.23E+05

Relative error (%): 1.7

Effective uranium content of monitor (ppm): 39

zeta factor & standard error (yr cm^2): 127 5

Size of counter square (cm^2): 1.39E-06

Grain	RhoS	Ns	RhoI	Ni Squares		U	±2s	Grain age (Ma)	
no.	(cm^-2)	(cm^-2)		(ppm)			±95%	CI--	
1	1.30E+07	217	8.42E+05	14	12	63	33	490	293.1
	893.4								
2	1.80E+06	15	4.69E+06	39	6	350	112	12.8	6.5
	23.7								
3	7.22E+05	12	4.87E+06	81	12	363	81	5	2.4
	9.1								
4	4.33E+05	9	6.88E+06	143	15	513	87	2.1	0.9
	4.1								
5	4.01E+05	10	4.17E+06	104	18	311	62	3.2	1.5
	6.1								
6	4.51E+06	50	2.62E+06	29	8	195	72	56.9	35.4
	93.3								
7	4.33E+05	9	4.76E+06	99	15	355	72	3.1	1.3
	6								
8	9.20E+06	102	2.53E+06	28	8	188	71	119.4	78.4
	188.4								
9	6.67E+06	111	3.67E+06	61	12	273	70	60.1	43.6
	83.6								
10	1.69E+07	187	5.50E+06	61	8	410	106	100.8	75.3
	137.1								
11	9.62E+05	12	4.33E+06	54	9	323	88	7.5	3.6
	14								
12	1.44E+05	3	3.03E+06	63	15	226	57	1.7	0.3
	4.8								
13	3.61E+05	14	3.27E+06	127	28	244	44	3.7	1.9
	6.4								
14	6.13E+05	17	4.33E+06	120	20	323	60	4.7	2.7
	7.9								
15	1.27E+07	212	3.19E+06	53	12	238	65	131.2	97
	180.9								
16	8.42E+05	14	4.69E+06	78	12	350	80	6	3.1
	10.6								
17	9.48E+05	46	7.30E+06	354	35	544	61	4.3	3.1
	5.9								
18	1.18E+07	163	4.33E+05	6	10	32	25	824.2	393
	2109.9								
19	5.77E+05	8	7.50E+06	104	10	560	111	2.6	1.1
	5.2								
20	2.02E+06	28	6.28E+06	87	10	468	101	10.7	6.7
	16.5								
21	2.41E+05	4	1.74E+06	29	12	130	48	4.7	1.2
	13								

22	1.38E+06	23	7.58E+06	126	12	565	102	6.1	3.7
	9.5								
23	1.60E+05	4	4.81E+06	120	18	359	66	1.2	0.3
	2.9								
24	5.77E+05	8	7.07E+06	98	10	527	108	2.8	1.1
	5.6								
25	1.32E+06	11	4.69E+06	39	6	350	112	9.5	4.3
	18.6								
26	3.38E+05	15	4.60E+06	204	32	343	49	2.5	1.3
	4.1								
27	6.61E+05	11	5.59E+06	93	12	417	87	4	1.9
	7.4								
28	6.01E+05	10	2.47E+06	41	12	184	57	8.2	3.6
	16.4								
29	4.81E+05	6	6.49E+06	81	9	484	109	2.5	0.9
	5.6								
30	2.25E+05	5	5.46E+06	121	16	407	75	1.4	0.4
	3.3								
31	6.73E+06	56	5.53E+06	46	6	412	122	40.3	26.8
	60.9								
32	2.89E+05	8	7.36E+06	204	20	549	79	1.3	0.6
	2.6								
33	1.60E+05	2	4.57E+06	57	9	341	91	1.3	0.1
	4.4								
34	1.23E+07	136	2.62E+06	29	8	195	72	153.2	102.7
	237.2								
35	9.02E+04	3	4.69E+06	156	24	350	57	0.7	0.1
	1.9								
36	2.58E+05	5	3.66E+06	71	14	273	65	2.4	0.7
	5.7								
37	3.37E+05	14	6.78E+06	282	30	506	63	1.7	0.9
	2.8								
38	3.61E+05	5	5.19E+06	72	10	387	92	2.4	0.7
	5.6								
39	5.05E+05	7	7.43E+06	103	10	554	111	2.3	0.9
	4.8								

HK3

Effective track density for fluence monitor (tracks/cm^2): 5.23E+05

Relative error (%): 1.7

Effective uranium content of monitor (ppm): 39

zeta factor & standard error (yr cm^2): 127 5

Size of counter square (cm^2): 1.39E-06

Grain	RhoS	Ns	RhoI	Ni Squares	U	±2s	Grain age (Ma)	
no.	(cm^-2)	(cm^-2)		(ppm)		±95%	CI--	
1	2.68E+06	52	1.08E+06	21	14	81	35	81.3	48.4
	142.3								
2	7.94E+05	11	4.91E+06	68	10	366	89	5.4	2.6
	10.2								

3	8.42E+05	14	6.55E+06	109	12	489	95	4.3	2.3
4	7.5 1.95E+07	189	4.43E+06	43	7	330	101	143.9	103.3
5	205.4 2.41E+05	2	2.28E+06	19	6	170	77	3.7	0.4
6	14.5 1.02E+06	17	5.89E+06	98	12	439	90	5.8	3.2
7	9.7 9.62E+05	16	6.67E+06	111	12	498	96	4.8	2.6
8	8.1 1.60E+05	2	1.84E+06	23	9	137	57	3.1	0.3
9	11.7 4.33E+06	36	1.08E+06	9	6	81	52	129.7	62.4
10	306.5 5.65E+06	47	3.25E+06	27	6	242	93	57.4	35.1
11	95.9 1.00E+07	139	5.27E+06	73	10	393	93	62.9	47
12	84.8 5.41E+05	9	5.77E+06	96	12	430	89	3.2	1.4
13	6.2 8.90E+06	111	6.01E+06	75	9	448	104	48.9	36.2
14	66.6 4.51E+05	5	3.70E+06	41	8	276	86	4.2	1.2
15	10.2 3.13E+06	52	2.65E+06	44	12	197	60	39.1	25.7
16	59.8 1.56E+06	13	9.14E+06	76	6	681	158	5.7	2.9
17	10.3 2.00E+05	5	1.88E+06	47	18	140	41	3.6	1.1
18	8.8 7.82E+06	65	4.81E+06	40	6	359	113	53.7	35.7
19	81.7 2.41E+05	3	1.92E+06	24	9	143	58	4.3	0.8
20	13.7 4.47E+05	13	2.44E+06	71	21	182	43	6.1	3.1
21	11.1 9.02E+04	3	7.22E+05	24	24	54	22	4.3	0.8
22	13.7 5.41E+05	15	4.15E+06	115	20	309	59	4.4	2.3
23	7.5 1.80E+06	25	3.46E+06	48	10	258	75	17.3	10.2
24	28.6 1.33E+07	111	2.41E+06	20	6	179	79	180.5	112.7
25	306.4 4.26E+06	59	9.38E+05	13	10	70	38	147.6	81.1
26	293.1 4.81E+05	10	2.50E+06	52	15	187	52	6.5	2.9
27	12.7 1.07E+07	89	3.61E+06	30	6	269	98	97.4	64.1
28	152.8 4.73E+05	21	5.01E+06	222	32	373	52	3.2	1.9
29	4.9 1.32E+05	11	6.61E+05	55	60	49	13	6.7	3.1
30	12.8 4.81E+05	14	5.43E+06	158	21	405	66	3	1.6
	5.1								

31	7.09E+06	59	3.01E+06	25	6	224	89	77.6	48.1
	129.5								
32	8.42E+06	140	2.83E+06	47	12	211	62	97.9	70.1
	139.5								
33	8.03E+06	89	2.80E+06	31	8	208	75	94.3	62.3
	147								
34	3.25E+05	9	3.54E+06	98	20	264	54	3.1	1.4
	6								
35	1.85E+07	256	3.82E+06	53	10	285	79	158.1	117.6
	216.7								
36	9.62E+05	12	8.66E+06	108	9	646	126	3.7	1.8
	6.7								
37	1.08E+05	3	1.70E+06	47	20	126	37	2.2	0.4
	6.6								
38	4.33E+05	12	3.07E+06	85	20	229	50	4.7	2.3
	8.6								
39	4.69E+05	13	4.58E+06	127	20	342	62	3.4	1.8
	6								
40	1.26E+07	174	4.47E+06	62	10	334	85	92.4	68.9
	125.7								
41	3.61E+05	12	5.41E+06	180	24	404	62	2.2	1.1
	4								
42	1.11E+07	92	2.28E+06	19	6	170	77	157.8	96.5
	273.6								
43	7.22E+04	2	9.02E+05	25	20	67	27	2.8	0.3
	10.7								
44	8.02E+05	10	7.05E+06	88	9	526	113	3.8	1.7
	7.3								
45	1.44E+06	16	7.12E+06	79	8	531	121	6.8	3.7
	11.6								
46	2.89E+05	6	3.37E+06	70	15	251	60	2.9	1
	6.5								
47	8.02E+05	20	5.21E+05	13	18	39	21	50.7	24.1
	110.9								
48	3.61E+05	8	3.97E+06	88	16	296	64	3.1	1.3
	6.2								
49	9.62E+05	20	4.86E+06	101	15	362	73	6.6	3.8
	10.7								
50	6.61E+05	11	5.11E+06	85	12	381	83	4.4	2.1
	8.1								
51	9.02E+05	10	4.33E+06	48	8	323	93	7	3.1
	13.9								
52	4.69E+05	13	1.41E+06	39	20	105	34	11.2	5.4
	21.2								
53	1.39E+07	116	4.09E+06	34	6	305	104	111.9	76.2
	169.3								
54	4.98E+06	69	8.95E+06	124	10	667	122	18.5	13.5
	25								

HK4

Effective track density for fluence monitor (tracks/cm^2): 5.23E+05

Relative error (%): 1.7

Effective uranium content of monitor (ppm): 39

zeta factor & standard error (yr cm^2): 127 5

Size of counter square (cm^2): 1.39E-06

Grain	RhoS	Ns	RhoI	Ni Squares		U	±2s	Grain age (Ma)	
no.	(cm^-2)	(cm^-2)		(ppm)			±95%	CI--	
1	1.39E+07	116	3.49E+06	29	6	260	96	130.9	87.1
	204.1								
2	3.61E+05	15	1.61E+06	67	30	120	30	7.5	3.9
	13.2								
3	1.92E+06	64	9.29E+06	309	24	693	82	6.9	5.2
	9.2								
4	5.41E+05	9	5.47E+06	91	12	408	86	3.3	1.5
	6.5								
5	1.44E+05	3	2.31E+06	48	15	172	50	2.2	0.4
	6.4								
6	9.02E+05	25	6.35E+06	176	20	473	73	4.7	3
	7.2								
7	6.01E+05	10	3.25E+06	54	12	242	66	6.2	2.8
	12.2								
8	6.73E+05	14	6.06E+06	126	15	452	82	3.7	2
	6.4								
9	2.16E+05	9	2.07E+06	86	30	154	34	3.5	1.5
	6.9								
10	1.12E+07	186	1.50E+06	25	12	112	45	241.1	160
	380.7								
11	8.84E+05	49	6.35E+06	352	40	473	53	4.6	3.3
	6.3								
12	5.29E+05	11	6.30E+06	131	15	470	83	2.8	1.4
	5.2								
13	1.53E+06	51	7.70E+06	256	24	574	74	6.6	4.8
	9								
14	4.81E+05	10	2.74E+06	57	15	204	54	5.9	2.7
	11.5								
15	8.37E+06	116	3.17E+06	44	10	237	71	86.8	61
	125.8								
16	3.97E+05	11	4.04E+06	112	20	301	58	3.3	1.6
	6.1								
17	3.01E+05	5	4.21E+06	70	12	314	76	2.4	0.7
	5.8								
18	4.24E+06	47	5.32E+06	59	8	397	104	26.4	17.6
	39.4								
19	4.12E+05	12	1.02E+07	297	21	761	92	1.4	0.7
	2.4								
20	1.07E+07	134	5.37E+06	67	9	401	98	66	48.9
	90								
21	9.74E+06	81	5.29E+06	44	6	395	119	60.7	41.6
	89.9								
22	6.61E+05	11	7.40E+06	123	12	551	101	3	1.4
	5.5								
23	1.02E+06	17	7.94E+06	132	12	592	105	4.3	2.4
	7.1								
24	7.22E+05	12	9.08E+06	151	12	677	112	2.7	1.3
	4.8								

25	6.49E+05	9	6.20E+06	86	10	463	101	3.5	1.5
	6.9								
26	6.01E+05	10	1.06E+07	176	12	789	122	1.9	0.9
	3.6								
27	2.26E+07	376	3.07E+06	51	12	229	64	239.7	179.5
	327								
28	1.01E+06	14	6.49E+06	90	10	484	103	5.2	2.7
	9.1								
29	8.30E+05	23	8.01E+06	222	20	597	83	3.5	2.1
	5.3								
30	4.21E+05	7	4.51E+06	75	12	336	78	3.2	1.2
	6.7								
31	5.41E+05	9	7.09E+06	118	12	529	99	2.6	1.1
	5								
32	4.21E+05	7	6.31E+06	105	12	471	93	2.3	0.9
	4.7								

HK5

Effective track density for fluence monitor (tracks/cm^2):	4.10E+05	
Relative error (%):		1.7
Effective uranium content of monitor (ppm):	39	
zeta factor & standard error (yr cm^2):	127	5
Size of counter square (cm^2):	1.39E-06	

Grain	RhoS	Ns	RhoI	Ni Squares		U	±2s	Grain age (Ma)	
no.	(cm^-2)	(cm^-2)		(ppm)			±95%	CI--	
1	1.32E+06	22	8.60E+06	143	12	818	139	4	2.4
	6.3								
2	5.67E+05	11	3.50E+06	68	14	333	81	4.3	2
	8								
3	1.66E+06	23	6.64E+06	92	10	631	133	6.5	3.9
	10.4								
4	1.23E+06	17	7.86E+06	109	10	748	145	4.1	2.3
	6.8								
5	1.80E+06	20	9.92E+06	110	8	944	182	4.8	2.8
	7.7								
6	4.81E+05	8	6.37E+06	106	12	606	119	2	0.8
	4								
7	6.25E+05	13	4.62E+06	96	15	439	91	3.6	1.8
	6.3								
8	1.20E+06	50	7.22E+06	300	30	686	83	4.4	3.1
	5.9								
9	1.38E+06	23	9.38E+06	156	12	892	146	3.9	2.4
	6								
10	9.02E+05	15	4.93E+06	82	12	469	104	4.8	2.5
	8.3								
11	9.02E+05	10	6.85E+06	76	8	652	151	3.5	1.6
	6.7								
12	1.89E+06	21	1.06E+07	118	8	1012	189	4.7	2.8
	7.4								
13	7.94E+05	11	6.78E+06	94	10	645	135	3.1	1.5
	5.7								

14	4.96E+05	11	3.88E+06	86	16	369	80	3.4	1.6
15	6.31E+05	7	4.33E+06	48	8	412	119	3.9	1.4
16	1.08E+06	15	7.65E+06	106	10	727	143	3.7	2
17	4.33E+05	9	3.22E+06	67	15	307	75	3.6	1.5
18	5.61E+05	7	4.57E+06	57	9	435	116	3.3	1.2
19	7.62E+05	19	4.01E+06	100	18	381	77	5	2.9
20	1.44E+06	16	7.94E+06	88	8	755	163	4.8	2.6
21	4.33E+05	6	4.33E+06	60	10	412	107	2.7	0.9
22	2.16E+05	6	1.98E+06	55	20	189	51	2.9	1
23	4.81E+05	10	7.55E+06	157	15	718	117	1.7	0.8
24	7.22E+04	3	1.25E+06	52	30	119	33	1.6	0.3
25	6.31E+05	7	4.69E+06	52	8	446	124	3.6	1.3
26	2.00E+05	10	2.04E+06	102	36	194	39	2.6	1.2
27	3.01E+05	5	2.22E+06	37	12	212	69	3.6	1.1
28	1.20E+06	25	6.49E+06	135	15	618	108	4.8	3
29	7.56E+05	22	7.04E+06	205	21	670	96	2.8	1.7
30	3.61E+05	7	2.83E+06	55	14	270	73	3.4	1.3
31	1.08E+06	21	1.07E+07	208	14	1020	145	2.6	1.6
32	1.37E+06	40	6.18E+06	180	21	588	90	5.8	4
33	7.50E+05	26	8.25E+06	286	25	785	97	2.4	1.5
34	3.97E+05	11	4.04E+06	112	20	384	74	2.6	1.2
35	9.62E+04	2	1.68E+06	35	15	160	54	1.6	0.2
36	2.89E+05	12	3.13E+06	130	30	297	53	2.4	1.2
37	7.22E+05	10	5.34E+06	74	10	508	119	3.6	1.6
38	1.01E+06	14	3.61E+06	50	10	343	97	7.3	3.7
39	1.72E+05	5	1.48E+06	43	21	141	43	3.1	0.9
40	7.22E+05	20	2.89E+06	80	20	275	62	6.5	3.8
41	2.89E+05	8	2.42E+06	67	20	230	57	3.2	1.3

42	1.80E+05	4	2.03E+06	45	16	193	58	2.4	0.6
43	6.4 2.71E+05	6	3.97E+06	88	16	377	81	1.8	0.6
44	4 8.82E+05	11	7.54E+06	94	9	717	149	3.1	1.5
45	5.7 1.56E+06	13	7.58E+06	63	6	721	183	5.4	2.7
46	9.9 1.92E+05	4	1.20E+06	25	15	114	45	4.3	1.1
47	12.1 2.45E+06	34	1.66E+07	230	10	1579	215	3.9	2.6
48	5.5 6.49E+05	18	6.13E+06	170	20	583	92	2.8	1.6
49	4.5 1.80E+05	5	1.52E+06	42	20	144	44	3.2	1
50	7.8 2.41E+05	6	6.81E+05	17	18	65	31	9.3	3
51	24.4 4.33E+05	9	3.85E+06	80	15	366	83	3	1.3
52	5.8 7.22E+05	8	7.22E+06	80	8	686	155	2.7	1.1
53	5.4 3.61E+05	5	3.61E+06	50	10	343	97	2.7	0.8
54	6.5 7.22E+05	15	4.38E+06	91	15	416	88	4.3	2.3
55	7.5 1.17E+06	26	6.13E+06	136	16	583	102	5	3.1
56	7.6 4.81E+05	10	2.41E+06	50	15	229	65	5.3	2.4
57	10.4 2.31E+06	48	1.29E+07	268	15	1226	155	4.7	3.3
58	6.4 1.53E+06	17	1.04E+07	115	8	987	187	3.9	2.2
59	6.4 7.22E+05	16	5.77E+06	128	16	549	99	3.3	1.8
60	5.5 6.41E+05	8	5.77E+06	72	9	549	130	2.9	1.2
61	6 7.94E+05	11	4.98E+06	69	10	474	115	4.2	2
62	7.9 5.61E+05	7	5.61E+06	70	9	534	128	2.7	1
63	5.7 8.66E+05	18	7.65E+06	159	15	727	118	3	1.7
64	4.8 5.86E+05	13	5.91E+06	131	16	562	100	2.6	1.3
65	4.6 1.48E+06	43	6.91E+06	201	21	657	95	5.6	3.9
66	7.8 2.53E+05	7	3.79E+06	105	20	360	71	1.8	0.7
67	3.7 1.44E+05	3	1.25E+06	26	15	119	46	3.1	0.6
68	9.8 5.84E+05	17	5.22E+06	152	21	497	82	2.9	1.7
69	4.8 8.59E+05	25	5.08E+06	148	21	484	81	4.4	2.8
	6.8								

70	3.25E+05	9	1.88E+06	52	20	178	50	4.6	2
	9.2								
71	1.20E+05	4	1.50E+06	50	24	143	41	2.2	0.5
	5.7								
72	1.80E+05	5	9.02E+05	25	20	86	34	5.3	1.6
	13.8								
73	7.22E+04	2	1.30E+06	36	20	124	41	1.6	0.2
	5.6								
74	3.46E+05	12	2.89E+06	100	25	275	56	3.2	1.6
	5.7								
75	1.35E+05	3	1.80E+06	40	16	172	54	2	0.4
	6.1								
76	6.73E+05	14	4.33E+06	90	15	412	88	4.1	2.1
	7.2								
77	3.37E+05	14	2.21E+06	92	30	210	44	4	2.1
	7								
78	4.12E+05	8	4.54E+06	88	14	431	93	2.4	1
	4.9								
79	1.20E+05	3	1.48E+06	37	18	141	46	2.2	0.4
	6.7								
80	1.98E+05	11	4.33E+06	240	40	412	55	1.2	0.6
	2.2								
81	1.44E+05	4	3.21E+06	89	20	305	65	1.2	0.3
	3.1								
82	5.77E+05	24	1.97E+06	82	30	188	42	7.7	4.6
	12.1								
83	1.98E+05	11	2.74E+06	152	40	261	43	1.9	0.9
	3.5								

SM1

Effective track density for fluence monitor (tracks/cm^2):	5.65E+05	
Relative error (%):		1.7
Effective uranium content of monitor (ppm):	36	
zeta factor & standard error (yr cm^2):	127	5
Size of counter square (cm^2):	1.39E-06	

Grain	RhoS	Ns	RhoI	Ni Squares	U	±2s	Grain age (Ma)	
no.	(cm^-2)	(cm^-2)		(ppm)		±95%	CI--	
1	8.66E+05	24	4.11E+06	114	20	262	50	7.6	4.6
	11.8								
2	1.88E+07	156	1.68E+06	14	6	107	56	384.1	227
	708.9								
3	1.44E+07	199	3.03E+06	42	10	193	60	167.4	120.1
	239.2								
4	8.85E+06	184	1.83E+06	38	15	116	38	170.9	120.7
	249								
5	2.40E+07	333	2.16E+06	30	10	138	50	384.7	267.8
	574.5								
6	2.57E+07	356	3.32E+06	46	10	211	62	271.2	200.4
	375.9								

7	7.22E+06	80	8.12E+05	9	8	52	34	306.6	157.8 685.9
8	2.65E+07	220	6.49E+06	54	6	414	113	144.3	107 198.1
9	3.13E+07	260	3.85E+06	32	6	245	86	284	198.1 421.9
10	1.09E+07	182	2.89E+06	48	12	184	53	134.4	97.6 188.7
11	2.40E+07	664	9.31E+06	258	20	593	76	91.6	77.7 108.1
12	1.37E+07	114	1.80E+06	15	6	115	58	264.7	156.5 485.2
13	8.76E+06	170	2.01E+06	39	14	128	41	154.1	108.8 224.1
14	1.23E+07	102	1.80E+06	15	6	115	58	237.4	139.6 437.3
15	2.48E+07	344	5.77E+06	80	10	368	83	151.8	117.7 195.6
16	1.46E+07	202	2.16E+06	30	10	138	50	236.2	161.8 358
17	2.07E+07	229	2.80E+06	31	8	178	64	258.7	178.9 388.1
18	1.24E+07	241	3.97E+06	77	14	253	58	110.9	84.9 144.8
19	1.21E+07	134	3.43E+06	38	8	218	71	125	87 184.2
20	4.29E+06	107	5.21E+05	13	18	33	18	285.8	163.3 549.4
21	2.18E+07	151	5.77E+06	40	5	368	116	133.7	94.2 194.5

SM1

Effective track density for fluence monitor (tracks/cm^2): 5.63E+05

Relative error (%): 1.7

Effective uranium content of monitor (ppm): 39

zeta factor & standard error (yr cm^2): 127 5

Size of counter square (cm^2): 1.39E-06

Grain	RhoS	Ns	RhoI	Ni Squares	U	±2s	Grain age (Ma)	
no.	(cm^-2)	(cm^-2)		(ppm)		±95%	CI--	
22	1.82E+07	202	1.71E+06	19	8	119	54	366.4	232.5 614.7
23	2.50E+07	208	2.41E+06	20	6	167	74	358.7	230 593.7
24	1.68E+07	209	2.41E+06	30	9	167	61	243.2	166.8 368.1
25	7.94E+06	176	1.17E+06	26	16	81	32	236.2	157.5 370.3
26	1.97E+07	382	2.16E+06	42	14	150	46	316	231.3 443.6

27	1.86E+07	258	1.80E+06	25	10	125	50	356.6	239.3
556.6									
28	1.20E+07	250	1.20E+06	25	15	83	33	345.8	231.9
540.4									
29	1.29E+07	179	1.73E+06	24	10	120	49	259.7	171
413.9									
30	1.53E+07	255	3.73E+06	62	12	258	66	144.5	108.5
192.2									
31	9.86E+06	82	3.25E+06	27	6	225	86	107.2	69
172.4									
32	4.45E+06	74	8.42E+05	14	12	58	31	184.5	104.8
352.8									
33	8.37E+06	116	2.53E+06	35	10	175	59	117	79.9
176									
34	1.90E+07	264	5.05E+06	70	10	350	84	132.7	101
174.3									
35	1.21E+07	101	1.68E+06	14	6	117	61	250.3	144.9
471.3									
36	7.64E+06	127	4.39E+06	73	12	304	72	61.8	46
83.7									
37	9.38E+06	78	2.04E+06	17	6	142	68	160.7	95.3
289.4									
38	2.06E+07	143	3.61E+06	25	5	250	99	200.2	131.4
318.8									
39	8.99E+06	187	2.93E+06	61	15	203	52	108.4	81
147.4									
40	1.36E+07	189	2.16E+06	30	10	150	55	220.3	150.6
334.6									
41	7.03E+06	78	3.52E+06	39	8	244	78	70.9	47.8
107.1									
42	9.50E+06	79	3.13E+06	26	6	217	84	107.2	68.5
174.1									
43	1.17E+07	324	2.99E+06	83	20	207	46	137.4	106.8
176.7									
44	9.50E+06	79	1.92E+06	16	6	133	66	172.7	101.3
316.1									
45	5.61E+06	140	2.28E+06	57	18	158	42	87	63.6
120.7									
46	2.58E+07	286	3.43E+06	38	8	237	77	262.5	188.2
377.3									
47	1.08E+07	270	3.53E+06	88	18	244	53	108.3	84.2
139.3									
48	1.05E+07	218	1.73E+06	36	15	120	40	212.1	149.6
310									
49	1.18E+07	163	3.17E+06	44	10	220	66	130.7	93.5
186.8									
50	6.22E+06	69	2.80E+06	31	8	194	69	78.8	51.1
124.7									
51	1.06E+07	88	4.21E+06	35	6	292	98	89	59.7
135.8									
52	8.66E+06	72	2.04E+06	17	6	142	68	148.5	87.6
268.6									
53	3.92E+06	87	6.76E+05	15	16	47	24	202.2	117.8
375.4									
54	1.09E+07	151	3.03E+06	42	10	210	65	126.9	89.9
183.1									

55	1.07E+07	133	2.81E+06	35	9	194	66	133.9	92.2
	200.3								
56	7.36E+06	102	3.61E+06	50	10	250	71	72.4	51.2
	103.8								
57	1.46E+07	162	7.40E+06	82	8	512	114	70	53.1
	92.3								
58	9.09E+06	126	2.74E+06	38	10	190	62	117.1	81.2
	173.1								
59	1.26E+07	140	3.70E+06	41	8	256	80	120.6	84.9
	175.2								
60	3.49E+06	58	1.44E+06	24	12	100	41	85.5	52.5
	143.9								
61	4.51E+06	75	1.02E+06	17	12	71	34	154.6	91.5
	279								
62	7.83E+06	76	2.99E+06	29	7	207	77	92.7	60
	147.5								
63	1.13E+07	125	2.53E+06	28	8	175	66	156.9	104.2
	245.4								
64	1.88E+07	156	3.01E+06	25	6	208	83	218	143.7
	346.2								
65	1.54E+07	171	5.77E+06	64	8	400	101	94.6	70.7
	128.3								
66	6.60E+06	64	1.13E+06	11	7	79	46	202.2	107.8
	423.4								
67	1.67E+07	232	3.97E+06	55	10	275	74	148.7	110.7
	203.3								
68	1.17E+07	195	3.55E+06	59	12	246	64	116.8	87.1
	159.2								
69	8.95E+06	62	5.77E+06	40	5	400	126	55.1	36.5
	84.2								
70	1.43E+07	159	2.89E+06	32	8	200	70	174.5	119.5
	263.3								
71	9.02E+06	75	3.61E+06	30	6	250	91	88.4	57.4
	140								
72	1.10E+07	228	4.33E+06	90	15	300	64	89.6	69.4
	115.7								
73	7.85E+06	87	1.26E+06	14	8	87	46	216.3	124.2
	410.1								

SM6

Effective track density for fluence monitor (tracks/cm^2):						5.63E+05			
Relative error (%):								1.7	
Effective uranium content of monitor (ppm):							39		
zeta factor & standard error (yr cm^2):							127	5	
Size of counter square (cm^2):							1.39E-06		
Grain	RhoS	Ns	RhoI	Ni Squares		U	±2s	Grain age (Ma)	
no.	(cm^-2)	(cm^-2)		(ppm)			±95%	CI--	
1	2.01E+07	251	4.65E+06	58	9	322	85	152.6	114.7
	206.8								

2	1.28E+07	213	2.53E+06	42	12	175	54	178.3	128.3 254.3
3	2.31E+07	256	4.51E+06	50	8	312	89	180.1	133.2 248.8
4	1.08E+07	135	2.49E+06	31	9	172	62	153.3	103.8 234.3
5	2.43E+07	202	4.33E+06	36	6	300	100	196.9	138.5 288.6
6	7.58E+06	105	3.10E+06	43	10	215	66	86.6	60.3 126.6
7	2.57E+07	214	4.93E+06	41	6	341	107	183.5	131.6 262.6
8	1.93E+07	214	3.07E+06	34	8	212	73	220.4	154.1 325.7
9	1.53E+07	212	1.80E+06	25	10	125	50	294.7	196.6 463
10	2.55E+07	353	7.36E+06	102	10	510	102	122.2	96.8 154.2
11	2.74E+07	380	6.49E+06	90	10	450	96	148.7	116.7 189.2
12	1.39E+07	231	6.61E+05	11	12	46	27	701.1	398.9 1370.6
13	9.88E+06	137	3.75E+06	52	10	260	72	93.4	67.5 131.2
14	2.54E+07	211	6.61E+06	55	6	458	124	135.5	100.6 185.8
15	1.01E+07	279	1.30E+06	36	20	90	30	270.4	192.2 392.4
16	1.93E+07	268	3.75E+06	52	10	260	72	181.3	134.8 248.8
17	1.54E+07	128	3.01E+06	25	6	208	83	179.6	117.4 287.4
18	1.72E+07	143	5.29E+06	44	6	366	111	114.9	81.7 165.1
19	9.92E+06	110	2.44E+06	27	8	169	65	143.5	94.1 227.3
20	1.26E+07	174	1.01E+06	14	10	70	37	425.4	252.6 781.6
21	1.52E+07	169	2.34E+06	26	8	162	63	227.2	151.2 356.7
22	2.03E+07	169	1.92E+06	16	6	133	66	363.9	221.8 643.6
23	1.68E+07	280	2.41E+06	40	12	167	53	244.8	176.5 349
24	2.39E+07	398	3.37E+06	56	12	233	63	247.5	185.9 329
25	1.64E+07	136	2.77E+06	23	6	191	79	206.9	133.7 336.4
26	1.47E+07	122	3.13E+06	26	6	216	84	164.9	108.1 262.1
27	2.24E+07	310	3.46E+06	48	10	240	69	226.3	167.5 312.9
28	2.50E+07	208	1.44E+06	12	6	100	57	584.7	338 1117.7
29	1.54E+07	128	3.25E+06	27	6	225	86	166.6	110.2 262.2

30	2.62E+07	290	4.87E+06	54	8	337	92	188.8	141.4
257.2									
31	1.23E+07	171	2.38E+06	33	10	165	57	182	125.7
272.5									
32	2.42E+07	336	4.55E+06	63	10	315	80	186.8	141.5
246.3									
33	2.59E+07	430	1.98E+06	33	12	137	48	448	318.3
652.7									
34	3.40E+07	283	1.44E+06	12	6	100	57	783.1	458.1
1472									
35	2.41E+07	200	1.80E+06	15	6	125	64	455.6	275.9
815.3									
36	2.74E+07	228	1.68E+06	14	6	117	61	551.9	331
1001.6									
37	1.86E+07	206	1.35E+06	15	8	94	48	468.8	284.2
837.8									
38	1.69E+07	211	3.53E+06	44	9	244	74	168.8	122.1
239									
39	1.09E+07	151	1.66E+06	23	10	115	48	229.3	148.8
371.3									
40	2.85E+07	237	2.89E+06	24	6	200	81	341.8	227.3
539.8									
41	1.23E+07	136	1.53E+06	17	8	106	51	277.7	169.8
487.3									
42	1.23E+07	205	3.31E+06	55	12	229	62	131.7	97.6
180.8									
43	4.69E+06	65	5.12E+06	71	10	355	85	32.7	22.9
46.4									
44	1.10E+07	610	4.00E+06	222	40	277	38	97.4	81.9
115.9									
45	1.06E+07	295	9.02E+05	25	20	62	25	406.5	273.9
631.8									
46	1.60E+07	133	2.65E+06	22	6	183	77	211.4	135.4
347.6									
47	2.42E+07	336	4.04E+06	56	10	280	75	210.6	159
284.4									
48	1.91E+07	238	1.36E+06	17	9	94	45	478.1	298.7
820.6									
49	1.82E+07	252	2.74E+06	38	10	190	62	232.1	165.7
334.8									
50	1.03E+07	143	8.80E+06	122	10	609	112	41.8	32.4
53.9									
51	1.30E+07	108	4.69E+06	39	6	325	104	98	67.6
145.4									
52	8.59E+06	119	1.59E+06	22	10	110	46	189.5	120.7
313									
53	2.91E+07	242	4.21E+06	35	6	291	98	241.7	170.4
354.1									
54	8.03E+06	89	1.25E+07	139	8	868	150	22.9	17.3
30.2									
55	1.05E+07	145	6.71E+06	93	10	465	97	55.4	42.2
72.7									
56	1.09E+07	106	3.20E+06	31	7	221	79	120.7	80.7
186.4									
57	2.19E+07	304	7.29E+06	101	10	505	102	106.4	83.9
135									

58	1.28E+07	178	4.69E+06	65	10	325	81	97.1	72.8
	131.1								
59	7.09E+06	59	4.57E+06	38	6	316	103	55.2	36.2
	85.4								
60	1.20E+07	199	6.79E+06	113	12	470	90	62.6	49
	79.9								
61	1.82E+07	151	3.37E+06	28	6	233	88	189.2	126.8
	293.6								
62	3.90E+06	54	2.45E+06	34	10	170	58	56.5	36.2
	89.5								
63	1.65E+07	228	4.33E+06	60	10	300	78	134.2	100.9
	181.6								
64	4.77E+06	119	6.81E+05	17	18	47	23	243.7	148.1
	430								
65	1.78E+07	296	3.19E+06	53	12	221	61	196.2	146.7
	267.8								
66	1.77E+07	246	3.03E+06	42	10	210	65	205.5	148.5
	291.8								
67	3.93E+06	49	4.81E+05	6	9	33	26	279.2	123.7
	785.2								
68	2.29E+07	318	4.04E+06	56	10	280	75	199.5	150.4
	269.7								
69	2.57E+07	214	6.01E+05	5	6	42	36	1335.5	615
	3568								
70	2.44E+07	203	3.25E+06	27	6	225	86	262.1	176.7
	405.7								
71	1.29E+07	215	2.41E+06	40	12	167	53	188.8	135
	271.3								

SM9

Effective track density for fluence monitor (tracks/cm^2):	5.63E+05	
Relative error (%):		1.7
Effective uranium content of monitor (ppm):	39	
zeta factor & standard error (yr cm^2):	127	5
Size of counter square (cm^2):	1.39E-06	

Grain	RhoS	Ns	RhoI	Ni Squares	U	±2s	Grain age (Ma)	
no.	(cm^-2)	(cm^-2)		(ppm)		±95%	CI--	
1	1.68E+07	209	1.76E+06	22	9	122	52	329	214.6
	532.1								
2	1.33E+07	166	6.33E+06	79	9	438	99	74.5	56.4
	98.4								
3	6.06E+06	84	8.95E+06	124	10	619	113	24.2	18.2
	32.3								
4	1.66E+07	230	2.60E+06	36	10	180	60	223.7	158.1
	326.5								
5	2.55E+07	247	6.70E+06	65	7	464	116	133.8	100.8
	177.3								
6	1.41E+07	195	2.38E+06	33	10	165	57	207.1	143.7
	308.7								

7	2.32E+07	257	8.12E+05	9	8	56	37	932.9	508.5 1938.1
8	1.46E+07	202	4.69E+06	65	10	325	81	109.6	82.1 146.3
9	1.05E+07	87	1.08E+06	9	6	75	49	331.6	171.5 738.1
10	2.68E+07	334	2.81E+06	35	9	194	66	331.2	235.7 480.8
11	1.16E+07	129	2.89E+06	32	8	200	70	142.1	96.4 216.2
12	2.35E+07	456	3.25E+06	63	14	225	57	252.2	192.3 330.2
13	1.07E+08	119	1.62E+07	18	1	1124	524	230.5	141.6 400.4
14	1.50E+07	166	2.71E+06	30	8	187	68	194.1	132 296.1
15	2.51E+07	209	1.68E+06	14	6	117	61	507.7	303.5 925.1
16	2.13E+07	177	7.70E+06	64	6	533	134	98	73.4 132.7
17	1.09E+07	91	1.92E+06	16	6	133	66	198.6	117.5 361
18	2.28E+07	284	1.08E+07	135	9	749	131	74.7	59.9 93
19	1.90E+07	158	8.42E+05	7	6	58	43	745	371.5 1774.2
20	2.60E+07	216	4.45E+06	37	6	308	101	204.8	144.9 298
21	5.95E+06	66	1.17E+06	13	8	81	44	177.3	98.4 349.6
22	4.25E+06	106	1.12E+06	28	18	78	29	133.4	87.8 210.2
23	2.09E+07	174	3.13E+06	26	6	216	84	233.8	155.8 366.6
24	2.15E+07	596	5.34E+06	148	20	370	62	142.1	116.8 172.9
25	1.81E+07	251	8.15E+06	113	10	564	108	78.8	62.2 99.7
26	7.32E+06	203	5.27E+06	146	20	365	62	49.5	39.4 62.1
27	1.97E+07	218	4.33E+06	48	8	300	87	160	117.1 223.4
28	1.53E+07	148	3.20E+06	31	7	221	79	167.9	114.1 255.6
29	1.42E+07	157	2.34E+06	26	8	162	63	211.4	140.2 332.7
30	1.49E+07	206	2.81E+06	39	10	195	62	185.6	132 268.2
31	2.18E+07	242	4.69E+06	52	8	325	90	164	121.5 225.6
32	1.39E+07	154	2.62E+06	29	8	181	67	186.4	125.7 287
33	1.57E+07	174	4.69E+06	52	8	325	90	118.3	86.6 164.6
34	1.01E+07	140	1.08E+06	15	10	75	38	322.4	192.5 585.6

35	1.43E+07	198	1.08E+06	15	10	75	38	451.2	273.2
	807.7								
36	3.03E+06	63	6.73E+05	14	15	47	25	157.6	88.5
	304.1								
37	1.11E+07	154	1.59E+06	22	10	110	46	244.1	157.4
	399.1								
38	2.29E+07	254	2.34E+06	26	8	162	63	338.4	228.5
	524.2								
39	1.59E+07	264	4.39E+06	73	12	304	72	127.5	97.4
	166.7								
40	1.73E+07	192	8.84E+06	98	8	612	125	69.5	53.8
	89.8								
41	1.14E+07	95	2.77E+06	23	6	191	79	145.3	92.1
	240								
42	1.66E+07	138	2.16E+06	18	6	150	70	266.5	164.9
	460.1								
43	9.20E+06	102	1.53E+06	17	8	106	51	209.5	126.3
	372.2								
44	7.65E+06	106	9.38E+05	13	10	65	35	282.2	161.2
	542.8								
45	1.86E+07	206	2.89E+06	32	8	200	70	225.3	155.9
	337								
46	1.76E+07	146	7.46E+06	62	6	516	132	83.6	61.7
	114.5								
47	3.67E+07	305	9.62E+06	80	6	666	150	134.3	103.9
	173.6								

Appendix A. Supplementary data 3.
U/Pb isotope ratios and age data for samples HK3 (Hsiukuluan) and SM6 (Shuimuting).

		Isotopic ratios						Ages (Ma)			
Grain	**^{207}Pb/ ^{235}U ±2s**	**^{206}Pb/ ^{238}U ratio**	**±1□**	**^{207}Pb/ ^{235}U ratio**	**±1□**	**^{207}Pb/ ^{206}Pb**	**±1□**	**^{206}Pb/ ^{238}U**	**±2□**	**^{207}Pb/ ^{206}Pb**	**±2□**
HK47	341.2	0.057	1.70	0.075	0.80	0.589	1.80	-386.9	324.0	465.5	4.9
HK48	2107.4	0.138	1.40	0.393	0.80	7.330	2.00	2093.4	35.4	2124.2	15.4
HK44	160.2	0.050	2.20	0.034	0.90	0.228	2.30	-519.5	528.1	207.5	3.3
HK37	1716.9	0.113	1.60	0.295	0.80	4.681	1.70	1787.0	82.9	1670.1	12.5
HK42	1814.6	0.118	1.80	0.320	0.80	5.213	2.00	1853.1	45.4	1774.3	13.7
HK41	145.5	0.050	2.80	0.029	1.00	0.206	3.00	-445.3	337.3	183.6	3.3
HK36	222.3	0.050	3.10	0.036	1.00	0.246	3.40	185.8	655.8	225.4	3.5
HK25	1798.4	0.120	2.40	0.345	1.00	5.646	3.00	1705.6	117.4	873.1	18.0
HK27	1776.5	0.121	2.60	0.345	1.00	5.711	3.20	1663.2	127.7	1879.7	19.3
HK30	1774.4	0.119	2.60	0.334	1.00	5.497	3.30	1706.4	84.5	1853.8	18.6
HK32	988.0	0.079	3.00	0.196	1.10	2.153	3.60	678.1	373.9	1144.2	13.3
HK26	2489.9	0.170	3.00	0.480	1.10	11.14	3.70	2474.4	201.1	2491.6	23.9
HK13	1433.4	0.095	3.30	0.266	1.10	3.427	4.00	1330.6	621.0	1501.0	16.4
HK9	178.7	0.058	3.70	0.034	1.20	0.264	4.40	205.8	1154.9	207.1	3.9
HK5	1731.4	0.115	4.40	0.293	1.40	4.612	5.60	1831.9	105.9	1660.8	21.1
HK17	1811.9	0.115	4.70	0.326	1.50	5.137	6.00	1813.4	101.0	1802.9	23.8
HK19	155.6	0.056	5.40	0.030	1.60	0.228	6.70	-327.8	279.8	191.8	4.4
HK14	341.2	0.057	1.70	0.075	0.80	0.589	1.80	-386.9	324.0	465.5	4.9
HK20	2107.4	0.138	1.40	0.393	0.80	7.330	2.00	2093.4	35.4	2124.2	15.4
SM1	2074.1	0.141	0.002	0.345	0.005	6.711	0.089	2244.9	24.45	1908.9	22.48
SM2	1760.9	0.109	0.001	0.311	0.004	4.665	0.057	1782.0	23.21	1746.3	19.67
SM3	1777.7	0.111	0.001	0.312	0.004	4.759	0.053	1812.9	21.07	1751.8	19.31

SM4		0.075	0.001	0.160	0.002	1.648	0.026	1069.0	32.58	955.6	11.83
	988.7	9.80									
SM5		0.065	0.002	0.126	0.002	1.124	0.027	764.6	51.97	767.5	10.94
	764.8	12.71									
SM6		0.052	0.002	0.023	0.000	0.163	0.005	285.6	76.40	145.2	2.36
	153.1	4.61									
SM7		0.110	0.001	0.287	0.004	4.325	0.048	1796.0	20.53	1626.4	18.10
	1698.1	9.06									
SM8		0.060	0.002	0.029	0.000	0.235	0.006	587.4	60.62	182.8	2.81
	214.4	5.19									
SM9		0.108	0.001	0.303	0.004	4.506	0.050	1772.4	20.72	1706.8	18.97
	1732.1	9.23									
SM10		0.060	0.002	0.024	0.000	0.199	0.006	594.1	64.02	155.1	2.45
	184.6	4.80									
SM11		0.098	0.002	0.280	0.004	3.737	0.062	1577.9	32.51	1588.9	20.07
	1579.3	13.33									
SM12		0.059	0.002	0.032	0.000	0.260	0.006	573.4	55.82	203.2	3.03
	234.4	5.17									
SM13		0.049	0.003	0.029	0.001	0.194	0.010	169.3	126.82	182.2	3.97
	180.2	8.85									
SM15		0.113	0.002	0.306	0.005	4.727	0.087	1846.2	34.68	1720.3	22.87
	1772.1	15.34									
SM17		0.075	0.003	0.049	0.001	0.500	0.016	1066.6	66.11	306.8	5.34
	411.7	10.64									
SM21		0.064	0.002	0.125	0.002	1.105	0.028	754.4	55.68	761.5	11.44
	755.9	13.67									
SM22		0.062	0.002	0.068	0.001	0.584	0.015	687.5	54.25	426.4	6.46
	467.3	9.32									
SM23		0.113	0.002	0.328	0.005	5.066	0.078	1844.8	27.57	1827.6	22.24
	1830.3	13.11									
SM26		0.115	0.002	0.325	0.005	5.114	0.088	1875.5	30.49	1813.8	22.92
	1838.4	14.60									
SM27		0.114	0.002	0.334	0.005	5.243	0.090	1870.4	30.16	1857.3	23.30
	1859.6	14.61									
SM28		0.116	0.003	0.338	0.006	5.388	0.123	1894.2	41.61	1879.3	27.14
	1882.9	19.57									
SM29		0.141	0.002	0.383	0.006	7.416	0.127	2237.0	28.54	2091.9	25.77
	2162.9	15.38									
SM30		0.058	0.002	0.073	0.001	0.578	0.018	511.9	69.42	454.2	7.52
	462.9	11.61									
SM31		0.117	0.002	0.311	0.005	5.019	0.091	1912.7	30.91	1747.9	22.35
	1822.6	15.31									
SM32		0.165	0.003	0.470	0.007	10.711	0.204	2512.2	30.67	2483.9	31.15
	2498.3	17.69									
SM33		0.116	0.002	0.296	0.004	4.737	0.090	1900.4	32.22	1669.0	21.77
	1773.9	15.92									
SM34		0.062	0.002	0.036	0.001	0.306	0.008	672.7	57.76	227.0	3.65
	271.3	6.51									
SM36		0.069	0.003	0.021	0.000	0.202	0.008	907.6	84.25	134.4	2.65
	186.6	6.92									
SM37		0.054	0.005	0.037	0.001	0.273	0.023	365.9	186.64	231.9	7.01
	245.2	18.32									
SM38		0.059	0.004	0.053	0.001	0.438	0.026	576.0	129.63	334.7	8.15
	368.5	18.44									
SM39		0.065	0.002	0.074	0.001	0.664	0.018	772.1	56.31	458.3	7.37
	516.9	11.26									

SM40		0.123	0.003	0.346	0.005	5.904	0.135	2000.1	37.36	1913.2	26.16
	1961.9	19.90									
SM42		0.134	0.003	0.330	0.005	6.173	0.154	2147.1	38.95	1839.6	25.93
	2000.7	21.82									
SM43		0.182	0.005	0.484	0.009	12.371	0.337	2674.0	41.14	2546.6	37.03
	2633.0	25.57									
SM44		0.067	0.003	0.031	0.001	0.288	0.011	823.0	77.88	196.1	3.73
	257.3	8.80									
SM49		0.127	0.003	0.371	0.006	6.704	0.203	2061.8	45.83	2033.8	30.37
	2073.1	26.72									
SM50		0.133	0.003	0.367	0.006	6.956	0.212	2138.4	45.15	2017.6	30.01
	2105.8	27.10									
SM51		0.074	0.006	0.005	0.000	0.049	0.004	1029.3	154.77	30.3	0.93
	49.0	3.74									
SM52		0.129	0.004	0.366	0.007	6.731	0.222	2079.0	49.25	2009.9	31.26
	2076.7	29.21									
SM62		0.136	0.004	0.341	0.007	6.870	0.286	2175.3	55.03	1890.6	31.41
	2094.7	36.86									